N,*N*′-Ethylenebis(pyridoxylideneiminato) and *N*,*N*′-Ethylenebis(pyridoxylaminato): Synthesis, Characterization, Potentiometric, Spectroscopic, and DFT Studies of Their Vanadium(IV) and Vanadium(V) Complexes

Isabel Correia,[a] João Costa Pessoa,*[a] M. Teresa Duarte,[a] Rui T. Henriques,[a] M. Fátima M. Piedade,[a] Luís F. Veiros,[a] Tamás Jakusch,[b] Tamás Kiss,*[b, c] Ágnes Dörnyei,[c] M. Margarida C. A. Castro,*[d] Carlos F. G. C. Geraldes,[d] and Fernando Avecilla[e]

Abstract: The Schiff base *N*,*N*′-ethylenebis(pyridoxylideneiminato) (H_2pyr_2en, **1**) was synthesized by reaction of pyridoxal with ethylenediamine; reduction of H_2pyr_2en with $NaBH_4$ yielded the reduced Schiff base *N*,*N*′-ethylenebis(pyridoxylaminato) (H_2Rpyr_2en, **2**); their crystal structures were determined by X-ray diffraction. The totally protonated forms of **1** and **2** correspond to H_6L^{4+}, and all protonation constants were determined by pH-potentiometric and ^1H NMR titrations. Several vanadium(IV) and vanadium(V) complexes of these and other related ligands were prepared and characterized in solution and in the solid state. The X-ray crystal structure of $[V^VO_2(HRpyr_2en)]$ shows the metal in a distorted octahedral geometry, with the ligand coordinated through the N-amine and O-phenolato moieties, with one of the pyridine-N atoms protonated. Crystals of $[(V^VO_2)_2(pyren)_2]\cdot 2H_2O$ were obtained from solutions containing H_2pyr_2en and oxovanadium(IV), where Hpyren is the "half" Schiff base of pyridoxal and ethylenediamine. The complexation of $V^{IV}O^{2+}$ and $V^VO_2^+$ with H_2pyr_2en, H_2Rpyr_2en and pyridoxamine in aqueous solution were studied by pH-potentiometry, UV/Vis absorption spectrophotometry, as well as by EPR spectroscopy for the $V^{IV}O$ systems and ^1H and ^{51}V NMR spectroscopy for the V^VO_2 systems. Very significant differences in the metal-binding abilities of the ligands were found. Both **1** and **2** act as tetradentate ligands. H_2Rpyr_2en is stable to hydrolysis and several isomers form in solution, namely *cis–trans* type complexes with $V^{IV}O$, and α-*cis*- and β-*cis*-type complexes with V^VO_2. The pyridinium-N atoms of the pyridoxal rings do not take part in the coordination but are involved in acid–base reactions that affect the number, type, and relative amount of the isomers of the $V^{IV}O$–H_2Rpyr_2en and V^VO_2–H_2Rpyr_2en complexes present in solution. DFT calculations were carried out and support the formation and identification of the isomers detected by EPR or NMR spectroscopy, and the strong equatorial and axial binding of the O-phenolato in $V^{IV}O$ and V^VO_2 complexes. Moreover, the DFT calculations done for the $[V^{IV}O(H_2Rpyr_2en)]$ system indicate that for almost all complexes the presence of a sixth equatorial or axial H_2O ligand leads to much more stable compounds.

Keywords: coordination modes · geometric isomers · N, O ligands · speciation · vanadium

[a] Dra. I. Correia, Dr. J. Costa Pessoa, Dra. M. T. Duarte, Dr. R. T. Henriques, Dra. M. F. M. Piedade, Dr. L. F. Veiros
Centro Química Estrutural
Instituto Superior Técnico, Av. Rovisco Pais, 1049-001 Lisboa (Portugal)
Fax: (+351) 21-846-4457
E-mail: pcjpessoa@popsrv.ist.utl.pt

[b] Dr. T. Jakusch, Prof. Dr. T. Kiss
Biocoordination Chemistry Research Group of the Hungarian Academy of Sciences
University of Szeged, P.O. Box 440, 6701 Szeged (Hungary)
Fax: (+36) 62-420-505
E-mail: tkiss@chem.u-szeged.hu

[c] Prof. Dr. T. Kiss, Á. Dörnyei
University of Szeged
Department of Inorganic and Analytical Chemistry, 6701 Szeged, P.O. Box 440 (Hungary)
E-mail: tkiss@chem.u-szeged.hu

[d] Dra. M. M. C. A. Castro, Prof. Dr. C. F. G. C. Geraldes
Departamento de Bioquímica da Faculdade de Ciências e Tecnologia
Centro de Neurociências, Universidade de Coimbra, 3000 Coimbra (Portugal)
Fax: (+351) 23-983-8512
E-mail: gcastro@ci.uc.pt

[e] Dr. F. Avecilla
Departamento de Química Fundamental
Universidade da Coruña, Campus de A Zapateira, 15071 A Coruña (Spain)

Supporting information for this article is available on the WWW under http://www.chemeurj.org/ or from the author. Some additional X-ray data for **1**, **2**, **4**, and **9** (SI-1); further discussion of IR spectra (SI-2); UV/Vis absorption data for the ligands and $V^{IV}O$ complexes prepared in this work (SI-3); determination of the dissociation constants of $[H_6R(pyr)_2en]^{4+}$ in aqueous solution by ^1H NMR Spectroscopy (SI-4); EPR spectra of solutions containing $V^{IV}O^{2+}$ and $H_2(pyr)_2en$ (SI-5); 2D NOESY, ROESY and TOCSY spectra (SI-6), information on experimental and calculated ^1H and ^{51}V NMR data (SI-7); determination of the pK_a values of the pyridine protons of complexes $[V^VO_2(Rpyr_2enH_n)]$ from ^1H and ^{51}V NMR (SI-8); some general information about the structures of $[M(Rpyr_2en)H_n]$ complexes ($M = V^{IV}O$, V^VO_2, and $n = 0$–2) calculated by DFT (SI-9); determination of the vanadium content in samples (SI-10); hydrolytic species of $V^{IV}O^{2+}$ and VO_2^+ and corresponding formation constants (SI-11).

 DOI: 10.1002/chem.200305317

Introduction

Vanadium is a bioessential element that is found in remarkably high concentrations in marine ascidians,[1] certain mushrooms,[2] and polychaete worms.[3] Three types of vanadium-containing enzymes are known: vanadium nitrogenases,[4] vanadium-dependent haloperoxidases,[5] and vanadium-containing nitrate reductases.[6,7] Among other biological effects, vanadium's insulin-like action[8] and anticancer activity[9] have stimulated a considerable amount of research. However, our understanding of the role of vanadium in living organisms is far from complete. For instance, in the insulin-like action, it is known that the originally supplied vanadium(IV) or vanadium(V) complexes undergo considerable transformations in the organism, including ligand-exchange processes and redox reactions, before participating in various phosphorylation/dephosphorylation reactions involved in the metabolism of glucose.[10] Most of vanadium's biologically important reactions occur in water-based environments such as blood plasma and intracellular fluids. Therefore the knowledge of the distribution and chemical speciation of the vanadium compounds in aqueous solution is of the utmost importance.

Several vanadium complexes of the Schiff base sal_2en {*N*,*N*′-ethylenediaminebis(salicylideneiminato)} and related ligands have been proposed as insulin-enhancing agents, and for the treatment of obesity and hypertension.[11,12] To date, only $[V^{IV}O(sal_2en)]$ has been tested in vivo for insulin-mimetic activity. Pyridoxal and pyridoxamine are forms of vitamin B_6, known cofactors required by many enzymes. They are nontoxic metabolites and fairly soluble in aqueous solution. Pyridoxal-containing vanadium complexes are therefore of potential therapeutic interest.

In this work we study the Schiff base derived from the condensation of pyridoxal with ethylenediamine: H_2pyr_2en (**1**; see Scheme 1). One disadvantage of Schiff bases (hereafter designated by SB) is their tendency to hydrolyze. This may yield the half SB (and one aldehyde), or proceed further to the ethylenediamine and a second molecule of pyridoxal. The complex $[(VO_2)_2(pyren)_2]\cdot 2H_2O$ was obtained from solutions containing H_2pyr_2en and $VOSO_4$, where Hpyren is the "half" SB **3** (see Scheme 1). However, this instability was overcome by reduction of the SB to give an amine: H_2Rpyr_2en (**2**). Both compounds **1** and **2** were isolated, characterized by X-ray diffraction, and their acid–base properties studied. H_2Rpyr_2en was found to be quite stable

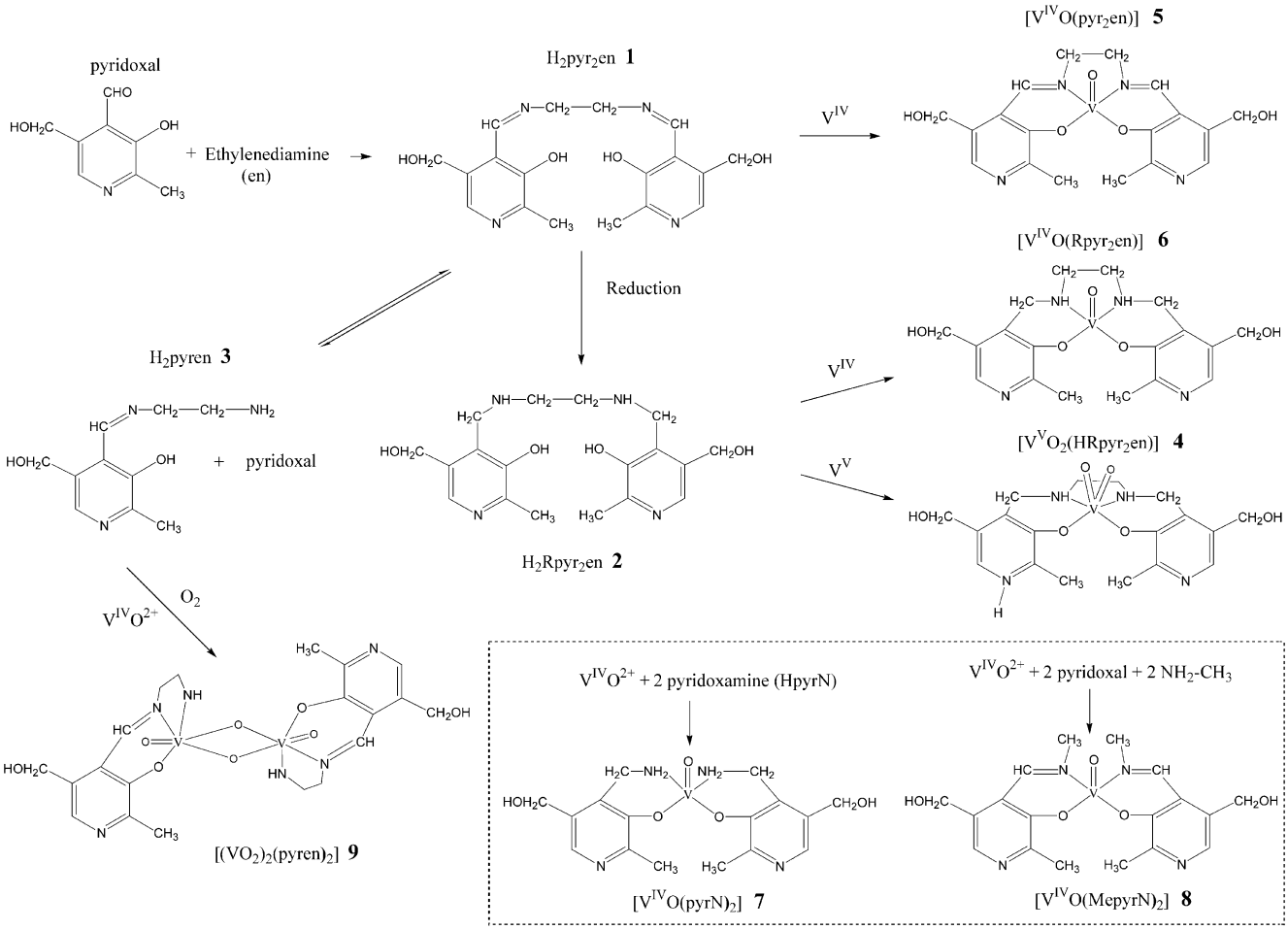

Scheme 1. Formulas of some of the compounds studied and their preparation. The H_2pyren (**3**) is designated as the half-Schiff base of **1**. This was only obtained as the ligand in $[(VO_2)_2(pyren)_2]\cdot 2H_2O$ (**9**).

to hydrolysis throughout the whole pH range. The vanadium(IV) complexes of the two ligands, of pyridoxamine (HpyrN) and of the SB derived from the reaction of methylamine with pyridoxal (HMepyrN) were synthesized and characterized in the solid state.

EPR, ^{1}H, and ^{51}V NMR spectroscopies were used to provide detailed information for the rather complicated solution equilibria of these ligands with $V^{IV}O^{2+}$ and $V^{V}O_2^{+}$. Ab initio[13] and DFT[14] calculations were carried out and support the formation and identification of the isomers present in both systems, and help to explain the experimental data. Overall the present systems are remarkable examples of the complexity of the types of isomers that may form in solutions of $V^{IV}O$ and $V^{V}O_2$ complexes (as indeed of many other metal–ligand systems), and how pH-potentiometry, spectroscopic techniques, DFT calculations, and computer handling of the experimental data may be used to characterize the systems in solution, and evaluate the various subtle effects that determine the isomers that form.

Results and Discussion

X-ray diffraction studies

H_2pyr_2en (1) and H_2Rpyr_2en (2): Figure 1 shows ORTEP representations of ligands H_2pyr_2en (**1**) and H_2Rpyr_2en (**2**). Only half of of **1** and **2** were found in the asymmetric unit, the inversion centers being located at the midpoint of the CH_2–CH_2 bonds. The overall geometrical parameters of H_2pyr_2en compare well with other ethylenebis(salicylideneimine) derivatives,[15–17] namely those of sal_2en[15] (see Table 1 for selected data). The N=CH and O–C lengths of **1** (1.277(5) and 1.349(5) Å, respectively) are consistent with the double-bond N=C and single-bond O–C character of these bonds, while the NH–CH_2 and O–C lengths of **2**

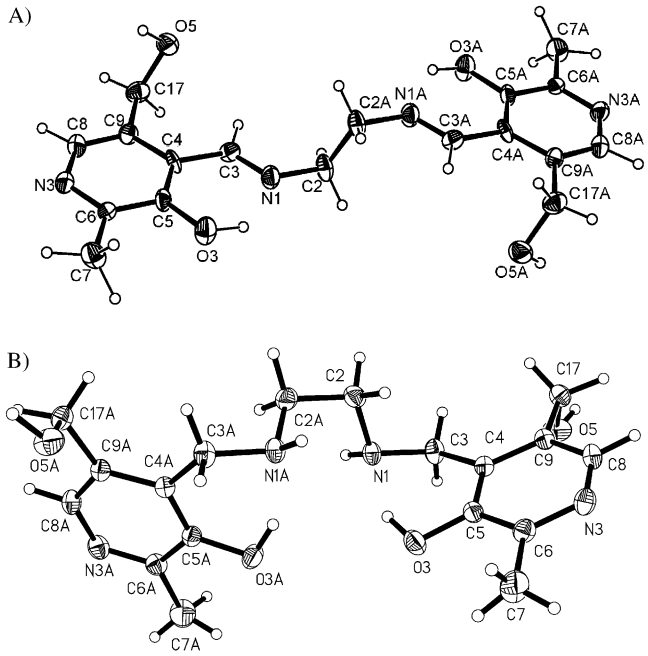

Figure 1. Structures of A) H_2pyr_2en (**1**) and B) H_2Rpyr_2en (**2**) (ORTEP diagrams; the thermal ellipsoids of the non-hydrogen atoms are drawn at the 30% probability level). There are short intramolecular hydrogen bonds: in **1** for O3–H3A···N1 (O···N 2.534(5) Å, H···N 1.69(8) Å, O–H···N 135(6)°), and in **2** for O3–H3···N1 (O···N 2.597(2) Å, H···N 1.71(3) Å, O–H···N 153(3)°). See also the Supporting Information (SI-1).

Table 1. Selected bond lengths [Å] and angles [°] for **1**, **2**, **4**, and **9**.

			$[V^{V}O_2(HRpyr_2en)]$ (**4**)			$[(V^{V}O_2)_2(pyren)_2]\cdot 2H_2O$ (**9**)[a]	
	H_2pyr_2en (**1**)	H_2Rpyr_2en (**2**)		X-ray	DFT		X-ray
N1–C2	1.464(6)	1.467(3)	V1–O1	1.628(5)	1.602	V1–O1	1.6026(19)
N1–C3	1.277(5)	1.471(2)	V1–O2	1.683(4)	1.614	V1–O2	1.6826(17)
O3–C5	1.349(5)	1.357(2)	V1–O3	1.897(4)	1.911	V1–O3	1.9088(19)
N3–C6	1.318(6)	1.333(2)	V1–O4	1.967(4)	2.103	V1–N2	2.127(2)
N3–C8	1.361(6)	1.339(3)	V1–N1	2.247(5)	2.377	V1–N1	2.155(2)
C3–C4	1.468(6)	1.509(2)	V1–N2	2.308(6)	2.433	V1–O2#1	2.3587(18)
C4–C9	1.410(6)	1.394(2)	O3–C5	1.320(7)	1.332	O3–C5	1.322(3)
C4–C5	1.392(6)	1.396(2)	O4–C12	1.314(7)	1.280	N2–C2	1.483(4)
C5–C6	1.401(5)	1.395(2)	N2–C10	1.471(8)	1.456	N1–C1	1.456(3)
O5–C17	1.425(7)	1.425(2)	N2–C1	1.470(9)	1.463	N1–C3	1.277(3)
C6–C7	1.487(6)	1.499(3)	N1–C3	1.482(9)	1.475	O1-V1-O2	107.33(10)
C8–C9	1.356(6)	1.375(2)	N1–C2	1.469(9)	1.468	O3-V1-N2	155.18(9)
C9–C17	1.500(6)	1.505(3)	N3–C6	1.330(8)	1.331	O2-V1-N1	154.92(8)
C2-N1-C3	119.3(5)	112.84(16)	N4–C13	1.333(8)	1.346	O3-V1-N1	82.92(8)
C6-N3-C8	119.1(5)	118.16(16)	N3–C8	1.355(9)	1.342	N2-V1-N1	76.90(8)
N1-C3-C4	120.0(5)	111.42(15)	N4–C15	1.335(8)	1.351	V1-O2-V1#1	101.84(8)
N3-C6-C5	120.6(5)	121.30(17)	O1-V1-O2	106.8(2)	109.8	O1-V1-O3	102.19(10)
N3-C6-C7	118.8(5)	117.70(18)	O1-V1-O3	100.6(2)	102.6	O2-V1-O3	99.17(8)
N3-C8-C9	124.1(5)	124.40(17)	O3-V1-O4	155.7(2)	148.4	O1-V1-N1	96.5(9)
			O2-V1-N1	164.2(2)	157.9	O1-V1-N2	94.39(11)
			O1-V1-N2	162.4(2)	160.8	O2-V1-N2	93.25(9)
			N1-V1-N2	74.4(2)	71.4	O1-V2-O2#1	171.47(8)
			O2-V1-O4	94.0(2)	92.9	O1-V1-O2#1	78.16(8)
			O4-V1-N1	81.54(19)	76.2		
			O3-V1-N1	80.99(19)	74.2		
			O4-V1-N2	76.9(2)			

[a] #1: $-x+2, -y, -z$

(1.471(2) and 1.357(2) Å, respectively) are consistent with their single-bond character. The configurations of **1** and **2** are determined by the strong intramolecular H bonds between $O_{phenolic}$–$N_{imine/amine}$. Their main differences are in the planarity of each half-molecule of H_2pyr_2en (planar within 0.012(3) Å), partly due to the conjugation of the C=N bond with the heteroaromatic ring. The two halves of **2** are nonplanar with respect to each other. For example the torsion angles C5-C4-C3-N1 and O3-C5-C4-C3 are −1.8(7)° and −0.3(7)° in the H_2pyr_2en, and 35.6(2)° and −2.3(3)° in H_2Rpyr_2en.

$[V^VO_2(HRpyr_2en)]\cdot 3H_2O$ (4): Upon coordination, the N_{amine} atoms become dissymmetric centers. The unit cell of the crystal contains four molecules: in two of them the configurations of the N_{amine} are *S,S*, while in the other two they are *R,R* (enantiomers of the *S,S* molecules). Figure 2A shows an

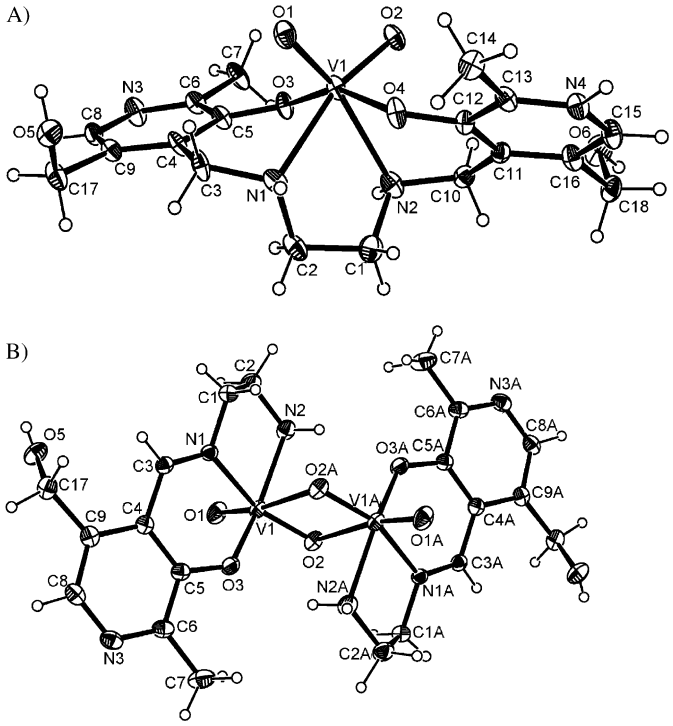

Figure 2. Structures of A) $[VO_2(HRpyr_2en)]\cdot 3H_2O$ (**4**) and B) $[(V^VO_2)_2(pyren)_2]\cdot 2H_2O$ (**9**) (ORTEP diagrams; the thermal ellipsoids are drawn at the 30% probability level). The H_2O molecules were not included. In (A) the N_{amine} atoms of the $[VO_2(HRpyr_2en)]$ molecule shown have *S,S* configuration. The binding mode involves two $O_{phenolate}$ oxygen atoms *trans* to each other. The ligand is protonated at the pyridine N4 atom. Protonation at N3 instead of N4 corresponds to the same molecule. However, for the isomer with the two $O_{phenolate}$ atoms *cis* to each other (one *trans* to the O_{oxo} atom), the two pyridine rings are no longer equivalent and protonation at N3 or N4 corresponds to two different isomers.

ORTEP diagram with the atom-labeling scheme, and selected bond lengths and angles are given in Table 1. The molecule is neutral with one of the pyridinium nitrogens protonated, and corresponds to the symmetrical isomer, sometimes designated by α-*cis* (see below).[18] In complex **4** the $HRpyr_2en^-$ ligand coordinates the VO_2^+ moiety by means of two phenolate-O^- and two amine-N atoms forming a quite distorted octahedral coordination polyhedron. This is due both to the specific constraints of the VO_2 fragment and to the tetradentate coordination, which imposes stereochemical strain, but overall the coordination geometry of this compound is rather similar to other monomeric V^VO_2 complexes.[18–23] The distortion is reflected in the coordination distances and angles and there are two short bonds (V=O bonds of 1.628(5) and 1.683(4) Å) that are *trans* to the two V–N long bonds of 2.308(6) and 2.247(5) Å. The O-V-O angle in the VO_2 moiety is similar to those previously reported for related complexes with nitrogen *trans* to the oxo groups, for example, the α-*cis* isomer of the EDTA complex[24] and β-*cis* isomer of the EDDA complex.[18] Other authors[25] also found a rather similar type of isomerism and used the notation *cis*- and *trans*-phenolates. Hereafter we will use the α-*cis* and β-*cis* notation; however, as will be clear below, in solution the V^V–$Rpyr_2en$ system is much more complex, because several α-*cis* and β-*cis* complexes form.

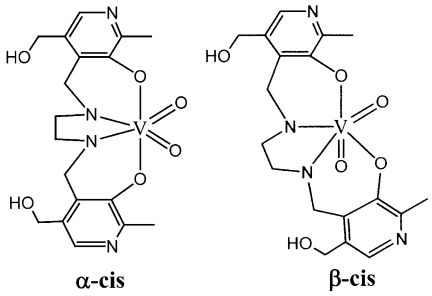

The differences observed in the V=O distances of $[V^VO_2(HRpyr_2en)]\cdot 3H_2O$ (**4**) are partly due to the different involvement of the two oxygen atoms in H bonding in the 3D structure. Atom O2 is involved in two short intermolecular H bonds (with N4 and O100 of two neighboring molecules), while atom O1 is only involved in a weaker one with O6 of a symmetry-related molecule.

General structures of the α-*cis* and β-*cis*-type complexes here: The V–$O_{phenolate}$ and V–N_{amine} bonds are within the normal range found for this type of compound.[20,25–28] The ligand coordinates vanadium forming a (6+5+6)-membered fused chelate system. The rings are not planar partly due to the greater flexibility of the reduced SB ligand, which is not constrained to remain planar when coordinated to the metal ion. Due to the fact that atom N4 is protonated and N3 is not, the two heteroaromatic rings have some differences namely: the N3–C8 and N4–C15 bonds, which differ by 0.014 Å, and some angles (e.g., C6-N3-C8 and C13-N4-C15 differ by 7.6°).

Comparing the bond lengths of ligand **2** and its complex, there are some small differences upon coordination; for example, the C–$O_{phenolic}$ bond decreases by 0.04 Å. However, there are no significant differences between the C3–N1 and C10–N2 internuclear separations.

$[(V^{V}O_2)_2(pyren)_2]\cdot 2H_2O$ (9): Although the initial mixture contained V^{IV} and H_2pyr_2en, a V^{V} complex with the half-Schiff-base monoanionic ligand Hpyren (**3**) was obtained, where one of the imine bonds hydrolyzed. The oxidation of V^{IV} was probably due to diffusion of air into the solution. An ORTEP diagram of **9** is shown in Figure 2B, and selected bond lengths and angles are in Table 1.

Compound **9** is a dinuclear V^{V} Schiff base with a bis(μ-oxo) bridge.[25,29–31] Each V^{V} ion is six-coordinate, and the μ-oxo atoms are *trans* to the V=O bonds. The coordination polyhedra obtained can be best described as two edge-shared octahedra that are significantly distorted. This distortion is mainly due to the O1-V1-O2 angle of 107.33(9)°, a value comparable to that obtained in compound **4** as well as in other VO_2 units found in the literature.[17,21–23,30–33] The V1–O1 bond has a typical V=O length of 1.6026(19) Å, while O2 is involved in the bridge between V1 and the symmetry-generated V1A atom ($-x+2$, $-y$, $-z$). This coordination gives rise to a rather distorted V_2O_4 core with two strong $V-O_{oxo}$ bonds, and two weak V–O interactions (see Table 1). The remaining three coordination sites are occupied by the tridentate $pyren^-$ units, comprising the phenolate-O3, the imine-N1, and the amine-N2 atoms. The metal is above the plane defined by N1, N2, O2, and O3 toward O1 by 0.354(1) Å. The V–V separation is 3.166(1) Å, comparable to the values found in related complexes that range from 3.103 Å to 3.372 Å.[30,31,33,34] Owing to the presence of two crystallization water molecules, there is an extended hydrogen-bonding network in the three-dimensional crystal structure, which involves both the bridging μ-oxygen atom O2, the hydroxyl O5 atom, and the pyridine N3 atom (see Supporting Information).

Infrared spectra: Some selected IR data for the ligands and vanadium complexes are shown in the Supporting Information. Some of the assignments were made based on literature data.[35–39] The characteristic ν(V=O) band appears as a medium-strong band at 960 cm^{-1} in the IR spectrum of $[V^{IV}O(pyr_2en)]$ (**5**), while for $[V^{IV}O(Rpyr_2en)]$ (**6**), the ν(V=O) band is shifted to much lower wavenumbers: 856 cm^{-1} (no other strong or medium-strong bands are seen in the 770–1000 cm^{-1} range). This low value is an indication of V=O···V=O interactions, in agreement with the magnetic susceptibility measurements (see below). The binding of an O_{oxo} to an adjacent vanadium atom, *trans* to its vanadyl-O atom, lengthens and weakens the bond, thereby lowering the V=O stretching frequency. For complexes **7** and **8** strong bands appear at 910 and 915 cm^{-1}, respectively, for the ν(V=O) stretches. These low values may also be an indication of V=O···V=O interactions as in **6**.

The IR spectrum of **4** is quite complex. This is partly due to the protonation at $N4_{pyridine}$, while $N3_{pyridine}$ is not protonated. This, and distinct hydrogen bonding, make several IR bands for equivalent group vibrations in each half of the ligand molecule appear at different wavenumbers. To help the assignment, the IR spectrum for a model compound of **4** was obtained from a DFT frequency calculation (see Supporting Information SI-2, and the Experimental Section). The bands at 1356(s) and 1290 cm^{-1} (medium-strong) are assigned to the $\nu(C12-O4)_{phenolate}$ and $\nu(C5-O3)_{phenolate}$, respectively. For the $V^{IV}O$ compounds these bands appear in the range 1273–1321 cm^{-1} (see Table SI-3 in the Supporting Information) and, in some cases, two bands may also be distinguished. The ν(V–O1) and ν(V–O2) bands were calculated to appear at 1001 and 974 cm^{-1}, while the experimental values are 924 and 903 cm^{-1}, respectively. The lower experimental values arise from the hydrogen bonding involving both O1 and O2.

Electronic absorption spectra: The electronic absorption spectra of bis(salicylaldimines) and of their transition-metal complexes have been extensively studied.[40–43] The electronic absorption spectra of the $V^{IV}O$ complexes (see Table SI-4 in the Supporting Information) were measured in DMSO. The $V^{IV}O$–Schiff base complexes **5** and **8** show a strong absorption with λ_{max} at 370–380 nm that is absent in the reduced Schiff base complexes. This band can be assigned to azomethine $\pi\rightarrow\pi^*$, but also has a contribution from a LMCT (phenolate-O to d orbitals on the vanadium) transition. Although three (or four) d–d bands are expected to appear in the absorption spectra of $V^{IV}O$ complexes, they are often overlapped or under strong CT bands. The spectrum of $[V^{IV}O(pyr_2en)]$ shows band I ($d_{xy}\rightarrow d_{xz}$, d_{yz}) at approximately 730 nm, and band II ($d_{xy}\rightarrow d_{x^2-y^2}$) at 580 nm. Band III ($d_{xy}\rightarrow d_{z^2}$) occurs below 500 nm and is under the much stronger band at ~380 nm. For complex **8**, band I is red-shifted but has about the same intensity as in **5**, and band II is blue shifted but less intense. In the 470–860 nm range the spectrum of $[V^{IV}O(Rpyr_2en)]$ is more intense than that of $[V^{IV}O(pyr_2en)]$. As expected the spectra of $[V^{IV}O(Rpyr_2en)]$ and $[V^{IV}O(pyrN)_2]$ are similar and the d–d bands I and II occur at about the same wavelength.

EPR spectra: The Hamiltonian parameters obtained by computer simulation of the experimental X-band EPR spectra of frozen solutions of the vanadium complexes in DMSO, using the computer program from Rockenbauer,[44] are listed in Table 2. The spectra of complexes **5**, **6**, and **8** show slight rhombic distortions, which can be seen in the perpendicular lines $M_1=7/2$, 5/2, and 3/2, indicating a distorted geometry around the metal center. The g_x-g_y values are in the range 0.005 to 0.009 while the $|A_x-A_y|$ are ~6 to 8×10^{-4} cm^{-1}. The degree of rhombic distortion increases in the order of complex **6**<**8**<**5**. In complex **6** the ligand is less rigid than in **5**, allowing the molecule to assume a more symmetric geometry around the metal center. In complexes **5** and **8** the ligands are Schiff bases, but in **8** instead of an ethylene bridge there are two methyl groups, which possibly explains the higher distortion in complex **5**. The additivity rule[45–48] was developed to allow the determination of the identity of the equatorial donor groups in complexes of square-pyramidal geometry (or octahedral with a weak sixth ligand), but has also been successfully applied to structurally distorted molecules.[49–51] The spectrum of **7** shows axial symmetry, and if we consider that the two ligand molecules bind vanadium in equatorial positions through the four donor atoms $(2\times N_{amine}, 2\times O_{phenolate})_{eq}$, the estimated A_z is 158×10^{-4} cm^{-1}. If the binding mode involves $(2\times O_{phenolate}, N_{amine},$

Table 2. Spin Hamiltonian parameters obtained by using a computer program from Rockenbauer.[44]

Compound		g_x, g_y	A_x, A_y ($\times 10^4$ cm^{-1})	g_z	A_z ($\times 10^4$ cm^{-1})
in DMSO					
$[V^{IV}O(pyr_2en)]$ (**5**)		1.985, 1.975	47.9, 55.7	1.956	157.8
$[V^{IV}O(Rpyr_2en)]$ (**6**)		1.979, 1.975	47.8, 53.6	1.957	157.5
$[V^{IV}O(pyrN)_2]$ (**7**)		1.977	54.1	1.954	162.2
$[V^{IV}O(Me\text{-}pyrN)_2]$ (**8**)		1.981, 1.976	48.5, 55.7	1.955	159.5
$[V^{IV}OSO_4]\cdot 5H_2O$		1.996, 1.976	34.5, 60.0	1.949[a]	167.7[a]
in water					
$[V^{IV}O(pyr_2en)(H_4)]$		n.d.	n.d.	~1.942	~172
$[V^{IV}O(H_npyr_2en)]$ ($n=2$–0)		1.982, 1.978	46.2, 56.2	1.956	158.7
$[V^{IV}O(H_nRpyr_2en)]$ (n = 2–0)[b]					
	pH 3.5–4.5	1.981	57.2	1.953	166.2
cis isomer[c]	pH 7.05	1.981	56.0	1.953	165.0
	pH 7.60	1.981	56.0	1.951	163.7
	pH 3.5–4.5	1.981	50.6	1.960	158.2
trans isomer[c]	pH 7.05	1.980	50.7	1.960	157.5
	pH 7.60	1.980	51.5	1.960	157.0
$[V^{IV}O(H_npyrN)]$ ($n=1,0$)		1.976	58.5	1.943	169.3
$[V^{IV}O(H_npyrN)_2]$ ($n=2$–0)		1.986	59.5	1.945	159.4

[a] If the binding mode of $[V^{IV}OSO_4]\cdot 5H_2O$ in DMSO involves four equatorial DMSO ligands, the contribution of each to the $g_\parallel$ and $A_\parallel$ values is $g_\parallel^{DMSO} \sim 0.487$ and $A_\parallel^{DMSO} \sim 42\times10^{-4}$ cm^{-1}, respectively. [b] Two distinct EPR active species are detected in aqueous solution. The composition of the solution according to the speciation: pH 3.5–4.5 100% $[V^{IV}OLH_2]$; pH 7.05 28% $[V^{IV}OLH_2]$, 56% $[V^{IV}OLH]$, 16% $[V^{IV}OL]$; pH 7.60 6% $[V^{IV}OLH_2]$, 46% $[V^{IV}OLH]$, 47% $[V^{IV}OL]$. [c] The *cis*- and *trans*-type isomers correspond to complexes where the H_2O ligand is *cis* or *trans* to the V=O group, respectively.

DMSO)$_{eq}$ (N_{amine})$_{ax}$, taking $A_\parallel(DMSO) = 42\times10^{-4}$ cm^{-1} (see Table 2), then the estimated parameters fit better with the simulated ones. This is probably the coordination mode of **7** in DMSO. For complexes **5, 6**, and **8** the EPR parameters (Table 2) fit well with the tetradentate binding mode involving either ($2\times N_{amine}$, $2\times O_{phenolate}$)$_{eq}$ or ($2\times N_{imine}$, $2\times O_{phenolate}$)$_{eq}$.

Magnetic properties of the vanadium(IV) complexes: The magnetic susceptibilities, χ, of the vanadium(IV) complexes **5** and **6** were measured by the Faraday method in the temperature range of 3–287 K. Data were corrected for the diamagnetic contribution using the Pascal constants.[52] The magnetic susceptibility of $[V^{IV}O(pyr_2en)]$ fits well the Curie–Weiss law (with $\chi_P(287\text{ K}) = 1.35\times10^{-3}$ emu mol^{-1}, $C = 0.381$ emu K mol^{-1}, $\theta = -0.32$ K). Yamada et al.[53] reported a μ_{eff} of 1.53 μ_B for this complex at room temperature (RT). However, we obtained a μ_{eff}(RT) of 1.76 μ_B (roughly constant until approximately 25 K), typical of monomeric $V^{IV}O$ compounds. This is in agreement with its green color and with the ν(V=O) value obtained. In contrast, for complex $[V^{IV}O(Rpyr_2en)]$, smaller μ_{eff}(RT) values were obtained: 1.50 μ_B, and these remain approximately constant until approximately 25 K. At low temperatures, an increase was observed, which suggests that ferromagnetic interactions become important. Low magnetic moments were found for several vanadium complexes[19,53–56] with sal_2en type ligands, and these low magnetic moments have been explained by the existence of V=O···V=O interactions. Possibly this is also the case for $[V^{IV}O(Rpyr_2en)]$, which is in agreement with the low ν(V=O) value for this complex (see above).

Ligand protonation by pH-potentiometry and ^{1}H NMR spectroscopy

pH-potentiometry: The H_2pyr_2en and H_2Rpyr_2en ligands contain six protons that dissociate in the measurable pH range, so the totally protonated species correspond to $[H_6pyr_2en]^{4+}$ and $[H_6Rpyr_2en]^{4+}$, respectively. The totally protonated pyridoxamine and pyridoxal correspond to $[H_3pyrN]^{2+}$ and $[H_2pyr]^+$, respectively. When referring to stoichiometries of complexes present in solution, the usual $M_pL_qH_r$ notation will be used, where L is the totally deprotonated form of the compounds, which corresponds to $[pyr_2en]^{2-}$, $[Rpyr_2en]^{2-}$, $[pyrN]^-$, and $[pyr]^-$. At very high pH (>12–13) the hemiacetal form of pyridoxal may also deprotonate yielding a species $[H_{-1}pyr]^{2-}$. The corresponding protonation constants are included in Table 3.

Schiff bases of the sal_2en type may hydrolyze in solution forming the half SB or eventually totally decompose at low pH,[57,58] and their $V^{IV}O$ complexes may be involved in disproportionation reactions.[59–61] All these processes depend on the solvent used. The H_2pyr_2en ligand is soluble in water, and much more stable in this solvent than sal_2en, and pH-potentiometry could be used to determine the protonation constants (see Table 3). No hydrolysis was detected in the pH range 2–7 by ^{1}H NMR spectroscopy, but at pH >7 a very weak signal corresponding to one of the aldehyde protons of pyridoxal could be detected. This slight extent of hydrolysis may explain the significantly higher uncertainties in the protonation constants of **1**, about twice those of H_2Rpyr_2en (**2**), which is also reasonably soluble in water but fairly stable throughout the pH range 1–13, as also confirmed by ^{1}H NMR spectroscopy. Table 3 also includes the protonation constants of pyridoxamine (obtained in this work), and those of pyridoxal.[62,63] For **2** and pyridoxamine the deprotonation processes overlap each other and the pK_a values were calculated from both the pH-metric and ^{1}H NMR data.

For pyridoxal the pK_{a1} of 12.9 corresponds to the deprotonation of its hemiacetal form,[62] and in the case of pyridoxamine the pK_{a1} of ~10.3 corresponds mainly to the amino group. In neutral aqueous solution the zwitterionic form predominates (the phenol deprotonated and the pyridine-N protonated), but a significant amount of the uncharged forms are also present; microequilibria must be considered. The pK_a of ~8 of pyridoxal and of pyridoxamine are largely associated with the pyridinium protons, and the pK_a of ~3–4 to both the hydroxyl and the pyridinium protons.[64] However, in the case of our ligands the existence of H bonds between the $O_{phenolic}$ and the $N_{amine/imine}$ may change further the

Table 3. Protonation and formation constants[a] of species $M_pL_qH_r$ formed in the V^VO_2–H_2Rpyr_2en and $V^{IV}O$–H_2pyr_2en, H_2Rpyr_2en and pyridoxamine systems calculated from the pH-potentiometric data with the PSEQUAD computer program,[63] and from ^1H NMR data (some pK_{ai} values).

	H_2pyr_2en		H_2Rpyr_2en		Pyridoxamine[b]	
	log β potentiometry	pK_a	log β	pK_a potentiometry [^1H NMR]	log β	pK_a potentiometry [^1H NMR]
HL	10.07(2)	10.07(2)	10.52(1)	10.52(1) [10.7(4)]	10.26(1)	10.26(1) [10.6(3)]
H_2L	18.86(3)	8.79(5)	19.67(1)	9.15(2) [8.9(4)]	18.25(1)	7.99(2) [8.1(1)]
H_3L	26.94(3)	8.08(6)	27.35(1)	7.68(2) [7.6(2)]	21.61(1)	3.36(2) [3.32(5)]
H_4L	33.83(4)	6.89(7)	33.33(1)	5.98(2) [5.5(2)]		
H_5L	38.26(5)	4.43(9)	36.37(2)	3.04(3) [–][c]		
H_6L	42.02(5)	3.76(10)	38.60(2)	2.23(4) [–][c]		
	log β ($V^{IV}O^{2+}$)		log β ($V^{IV}O^{2+}$)		log β ($V^VO_2^+$)	log β ($V^{IV}O^{2+}$)
MLH_4	36.46(5)		–		38.62(8)	–
MLH_3	–		–		36.98(5)	–
MLH_2	28.01(3)		32.97(1)		33.71(4)	–
MLH	23.07(3)		26.23(2)		26.40(4)	16.58(1)
ML	~17		18.64(2)		18.07(3)	11.07(4)
ML_2H_2	–		–		–	31.36(7)
ML_2H	–		–		–	25.31(2)
ML_2	–		–		–	17.73(12)
fitting[d]	6.1×10^{-3}		6.6×10^{-3}		1.01×10^{-2}	1.9×10^{-3}
no. of points	113		316		436	317

[a] For each $\log\beta_{pqr}$ value listed obtained by pH-potentiometry, the standard deviation obtained in the particular calculation corresponding to the values shown are included in (parentheses). To account for the range of $\log\beta_{pqr}$ values obtained in the several equilibrium models tested, each standard deviation may be multiplied by about three times the values presented. [b] For the similar compound pyridoxal, the protonation constants (at 25 °C and 1 M KCl) are: 12.93, 8.28, 4.00.[62] [c] From the ^1H NMR titrations only an average value for pK_{a5} and pK_{a6} could be obtained (1.98 ± 0.06)—see Supporting Information. [d] Difference between the experimental and the calculated titration curves expressed as the volume (mL) of titrant.

acidity of the phenolic-OH, the acid–base microequilibria becoming more complicated.

The pH-potentiometry technique allows the determination of the protonation constants of the ligands (Table 3), but cannot provide information on the sequence of protonation of their basic sites. The protonation of the N and O atoms generally result in a deshielding of the nonlabile H atoms attached to adjacent carbon atoms.[65] Therefore, a ^1H NMR titration study (δ versus pH) was carried out for **2**. This study did not yield the whole set of microequilibria involved, but gives information about the main groups involved for each calculated pK_a value—see Supporting Information (SI-4). One of the N_{amine} atoms is protonated first, $pK_{a1}^{NMR} = 10.7$, a value close to the 10.4 reported for pyridoxamine.[64] The second proton corresponds to the $NH_{pyridine}$ bound to the unprotonated end of the en moiety, with a pK_{a2}^{NMR} value of 8.9, close to those reported for pyridoxine (8.96), and 4-desoxypyridoxine (9.98), which have no protonated positively charged side chains, and have their $O_{phenolate}$ deprotonated.[64] The third proton corresponds to the other $NH_{pyridine}$ connected to the protonated end of the en moiety, with a pK_{a3}^{NMR} value of 7.6, that is close to the value obtained for pyridoxamine (7.99), which has a protonated positively charged side chain and the $O_{phenolate}$ deprotonated.[64] The fourth proton corresponds to the protonated N_{amine}, with a pK_{a4}^{NMR} value of 5.5. The fifth and sixth protonations correspond successively to each $OH_{phenolate}$, but could not be distinguished by the NMR titration experiment. From these pK_a values and the deprotonation sequence it is clear that in **2** the formation of H bonds between the phenolic-OH and the amino-NH is favorable (as found in the crystals of **2**, see above), the phenolic protons being quite acidic, even more than those of pyridoxamine.

For the SB **1**, the ^1H NMR titration study indicates that the deprotonation scheme is similar to that of H_2Rpyr_2en. The higher pK_a value is mainly associated to one of the imine groups, which is in agreement with values reported for the N-pyridoxylideneamino acidato SBs,[66,67] then comes the two $NH_{pyridine}$, followed by the second imine proton. The pKa values of ~3.7 and ~4.4 are mainly associated with the phenolic protons.

Vanadium(IV) complexes studied by pH-potentiometry, visible absorption, and EPR spectroscopy: Due to precipitation of the neutral complexes $[V^{IV}O(pyr_2en)]$, $[V^{IV}O(Rpyr_2en)]$ and $[V^{IV}O(pyrN)_2]$ the pH-metric data could not be evaluated above pH 5, 8, and 7, for the $V^{IV}O$–H_2pyr_2en, $V^{IV}O$–H_2Rpyr_2en, and $V^{IV}O$–HpyrN systems, respectively. The pH-metric data were evaluated with the computer program PSEQUAD,[63] with the assumption of 1:1 (and 2:1 ligand-to-metal ratio, in the case of HpyrN) complexes of different protonation states. The best fit between the experimental and the calculated titration curves was obtained with the set of constants shown in Table 3. The species distribution curves of the complexes formed are depicted in Figure 3.

In the $V^{IV}O$–H_2pyr_2en system, complex formation starts at pH 3 with the formation of $[V^{IV}OLH_4]$, where only half of the molecule is coordinated, that is, the binding mode is $(N_{imine}, O_{phenolate}, 2\times H_2O)_{eq}$ (structure **I**). $[V^{IV}OLH_2]$ forms through the coordination of the second half of the molecule. Further successive deprotonations of the pyridinium-NH^+ ion, which do not participate in the coordination, yield

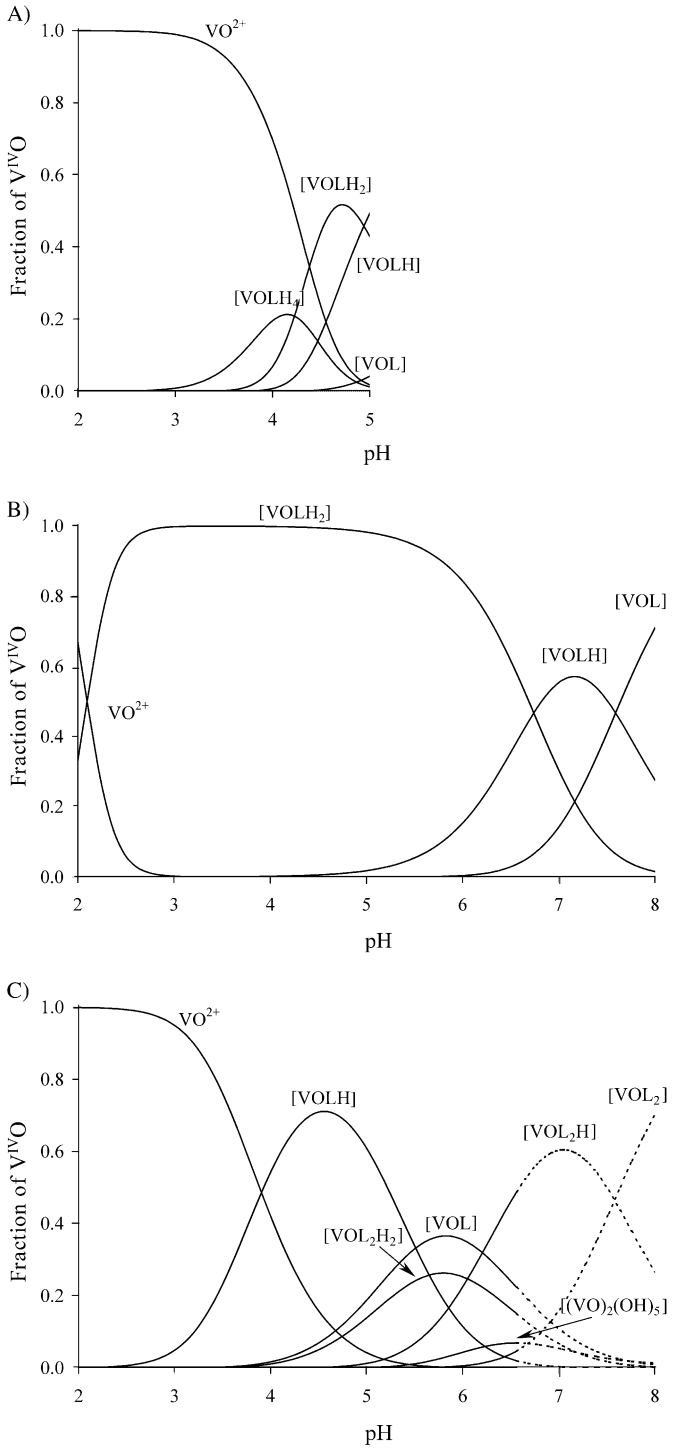

Figure 3. Concentration distribution curves of $V^{IV}O$ complexes formed in solutions containing A) $V^{IV}O^{2+}$ and H_2pyr_2en, with $C_{VO}=2.0$ mM and L:M = 2; B) $V^{IV}O^{2+}$ and H_2Rpyr_2en, with $C_{VO}=2.0$ mM and L:M = 2; and C) $V^{IV}O^{2+}$ and pyridoxamine, with $C_{VO}=1.0$ mM and L:M = 8.0, calculated by using the stability constants listed in Table 3 (L:M designates the ligand-to-metal ratio).

$[V^{IV}OLH]$ ($pK_a=4.9$) and $[V^{IV}OL]$ (neutral, $pK_a \sim 6.1$, corresponding to structure **II**), which is less soluble than [VOL] in the case of the $V^{IV}O$–H_2Rpyr_2en system.

In agreement with the speciation curves (Figure 3A), the spectra of solutions containing $V^{IV}O^{2+}$ and H_2pyr_2en start to deviate from that of $[V^{IV}O(H_2O)_5]^{2+}$ at pH > 3. As the pH is increased, the blue solutions become green and the bands at 370–470 nm ($\pi \rightarrow \pi^*$ imine and LMCT bands) develop further, indicating the coordination of both N_{imine} and $O_{phenolate}$ atoms. For the $V^{IV}O$–H_2Rpyr_2en system the changes in the visible spectra are also in agreement with the speciation model. At pH 1.8 the spectrum consists of a broad d–d transition band at 775 nm, a shoulder at about 680 nm (due to the aqua vanadyl ion), and a band at about 555 nm, showing that a significant amount of $[V^{IV}OLH_2]$ is present at this pH. Between pH 3 and 4.5 all the oxovanadium(IV) is in the form of $[V^{IV}OLH_2]$ and there are no spectral changes.

Figures 4 and SI-6 in the Supporting Information depict the high-field region of the X-band EPR spectra of frozen aqueous solution samples of the $V^{IV}O$–H_2Rpyr_2en and

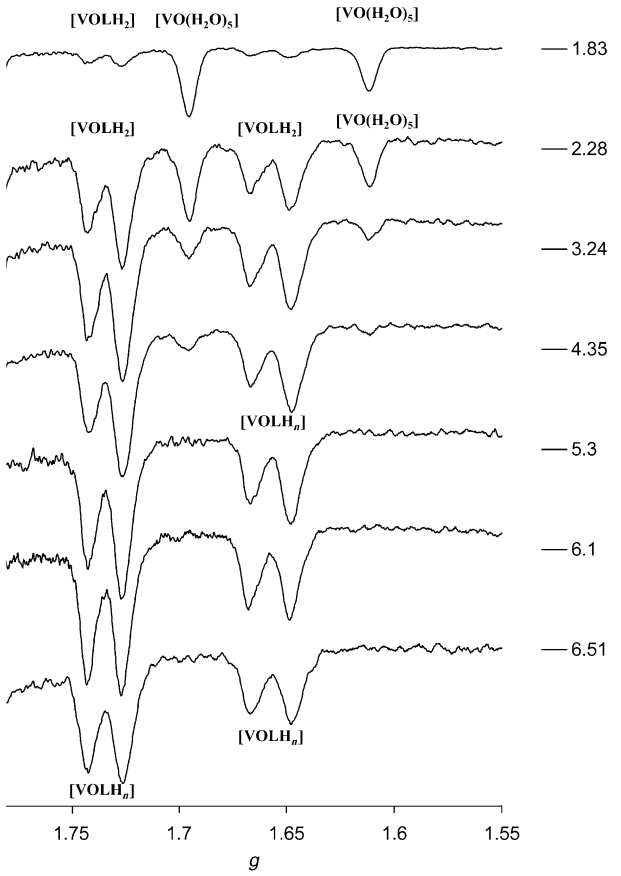

Figure 4. High-field region of the EPR spectra of frozen solutions (77 K) containing $V^{IV}O^{2+}$ and H_2Rpyr_2en at several pH values with L:M = 1 and $C_{VO} \sim 0.005$ M. The presence of two distinct components for the stoichiometries $[V^{IV}OLH_2]$, $[V^{IV}OLH]$, and $[V^{IV}OL]$ is clearly seen.

$V^{IV}O$–H_2pyr_2en systems, and Table 2 summarizes the EPR parameters obtained from the simulation of the spectra.[44] For the $V^{IV}O$–H_2pyr_2en system the experimental $A_{\parallel}$ value for $V^{IV}OLH_4$ fit well with the values estimated for a binding mode (N_{imine}, $O_{phenolate}$, $2\times H_2O)_{eq}$—structure **I**. Upon binding of the remaining part of the molecule, the processes $[V^{IV}OLH_2]^{2+} \rightarrow [V^{IV}OLH]^{+} \rightarrow [V^{IV}OL]$ involve only the deprotonation of the pyridinium-NH^+ ion. These groups do not participate in the coordination, and thus, no changes in

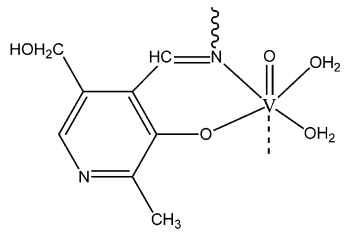

I

$A_{\parallel}^{est} \sim 170 \times 10^{-4}\ cm^{-1}$; $g_{\parallel}^{est} \sim 1.943$

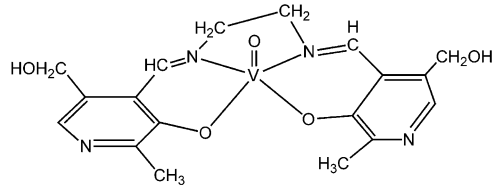

II

$A_{\parallel}^{est} \sim 158 \times 10^{-4}\ cm^{-1}$; $g_{\parallel}^{est} \sim 1.953$

the EPR spectra are observed. The rhombic distortion of the spectra, (e.g., Figure SI-6B in the Supporting Information), is an indication of the distorted environment around the vanadyl center, due to the rigid structure of the ligand.

Figure 3B shows that for the $V^{IV}O$–H_2Rpyr_2en system the complexation starts at pH 2, with the formation of $[V^{IV}OLH_2]^{2+}$. Further deprotonation yields $[V^{IV}OLH]^{+}$ and $[V^{IV}OL]$, which then precipitates. The EPR spectra, for example, Figure 4, show that for each stoichiometry two well separated signals can be ascribed. Evaluated from the intensities of the $M_I = 5/2$ and 7/2 components, the relative amount of the complexes is approximately the same in the pH range 2–5, suggesting that they are structural isomers. An H_2O ligand may coordinate in an equatorial position (*cis* to the $O_{vanadyl}$ atom) or axial (*trans* to the $O_{vanadyl}$ atom), as is common for $[V^{IV}OL_2]$ complexes, L being a bidentate ligand.[69,71] However, the type and number of isomers that may form in the present systems is complex, and a more systematic and comprehensive discussion about the stoichiometries and isomers that may form in solution is given below in connection with the DFT calculations.

In the $V^{IV}O$–HpyrN system (note that $pyrN^{-} \approx {}^1/_2[Rpyr_2en]^{2-}$), complex formation starts at pH ~2.5 with the formation of $[V^{IV}OLH]^{2+}$ (see Figure 3C), with a binding mode similar to that shown in structure **I** (with N_{amine} instead of N_{imime}). Deprotonation of the noncoordinated $NH^{+}_{pyridine}$ of this complex yields $[V^{IV}OL]^{+}$, while coordination of a second pyrN leads to the formation of $[VOL_2H_2]^{2+}$. Further deprotonation of the $NH^{+}_{pyridine}$ of the bis complex yields $[V^{IV}OL_2H]^{+}$ and $[V^{IV}OL_2]$, the latter is neutral and precipitates. The EPR spectra for this system (Table 2) indicate the presence of three distinct types of species in the pH range 2–6: the aqua vanadyl ion, $[V^{IV}OLH_m]$ and $[V^{IV}OL_2H_n]$. The simulated $A_{\parallel}$ value for $[V^{IV}OLH_m]$ fit well with the estimated value for the binding mode (N_{amine}, $O_{phenolate}$, $2\times H_2O)_{eq}$. Deprotonation of this species corresponds to only a slight decrease in the $A_{\parallel}$ values. In agreement with the proposed ($2\times N_{amine}$, $2\times O_{phenolate})_{eq}$ binding mode the spectra of $[V^{IV}OL_2H_n]$ correspond to lower $A_{\parallel}$ values than those of $[V^{IV}OLH_m]$. The linewidths and shape of the $M_I = 7/2$ components of the spectra indicate the existence of structural isomers also in this system. The visible spectra of the $V^{IV}O$–pyrN system show a pattern somewhat similar to those of the previous systems: as the pH increases the d–d transition at $\lambda_{max} \sim 760$ nm shifts to lower energy, and the one at $\lambda_{max} \sim 570$ ($\varepsilon = 12.9\ M^{-1}\ cm^{-1}$) shifts to higher energy. The intensity of both bands progressively increases.

Vanadium(V) complexes studied by pH-potentiometry, and ^1H and ^{51}V NMR spectroscopy: The ligand H_2pyr_2en does not form complexes with V^{V} stable enough to allow the use of pH-potentiometry. However, in the ^{51}V NMR spectra of solutions containing 3 mM of V^{V} and 6 mM of **1**, a new signal at $\delta \sim -577$ ppm was detected in the pH range 5–9, indicating complex formation. With pyridoxamine, the ^{51}V NMR measurements with 3 mM V^{V} and 12 mM of ligand did not show any complex formation in the same pH range. In the V^{V}–H_2Rpyr_2en system pH-potentiometry clearly indicated complex formation, and the stability constants given in Table 3 were obtained by the evaluation of the pH-metric titration data. The corresponding speciation diagram is shown in Figure 5.[70] At pH > 3.5, complexes $[VO_2LH_2]^{+} \rightarrow [VO_2LH] \rightarrow [VO_2L]^{-}$ are the predominant species with increasing pH, and at pH > 9.5 the ligand molecule is displaced from the coordination sphere and the oxoanions HVO_4^{2-}/VO_4^{3-} are formed. As in the $V^{IV}O$–H_2pyr_2en and $V^{IV}O$–H_2Rpyr_2en systems, these deprotonation processes involve the $NH^{+}_{pyridine}$ protons, and **2** acts as a tetradentate ligand in $[V^{V}O_2LH_2]^{+}$, $[V^{V}O_2LH]$, and $[V^{V}O_2L]^{-}$ (see below).

Between pH 3.5 and 6 the ^{51}V NMR spectra show only two relatively broad signals (Figure 6A and SI-7 in the Supporting Information). In the pH range 6–9, as the $NH^{+}_{pyridine}$ groups successively deprotonate, the two peaks gradually shift, but the ratios of the peak areas are almost independent on both the total V concentration or the L:M ratio. This indicates the formation of two mononuclear complexes for each stoichiometry, that is, structural isomers. There are two types of structural isomers (structures **III** and **IV** in Scheme 2), and for structure **IV** (β-*cis* isomer) the protons of the two half-molecules are not equivalent.

Separate ^1H NMR resonances are observed for the two isomers, due to slow exchange conditions, this being especially clear for the aromatic pyridoxal protons (e.g., signals assigned as α-*cis* and β-*cis* in Figure 6B). The assignments of all the other ^1H signals were confirmed by using 2D COSY spectra. Comparing the ^{51}V NMR spectra with the aromatic region of the ^1H NMR spectra (at 1:1 and other metal-to-ligand ratios, for example, Figure 6A , Figure 6B and SI-4 in the Supporting Information), and taking into account the relative areas of the NMR peaks, we conclude that while in the α-*cis* complex the two aromatic protons are equivalent, in the β-*cis* they correspond to two separate signals. This also occurs with the other pyridoxal protons (of CH_3, CH_2OH, and CH_2N), as well as with the en bridge -CH_2–CH_2- protons. This data supports structures **III** and **IV**

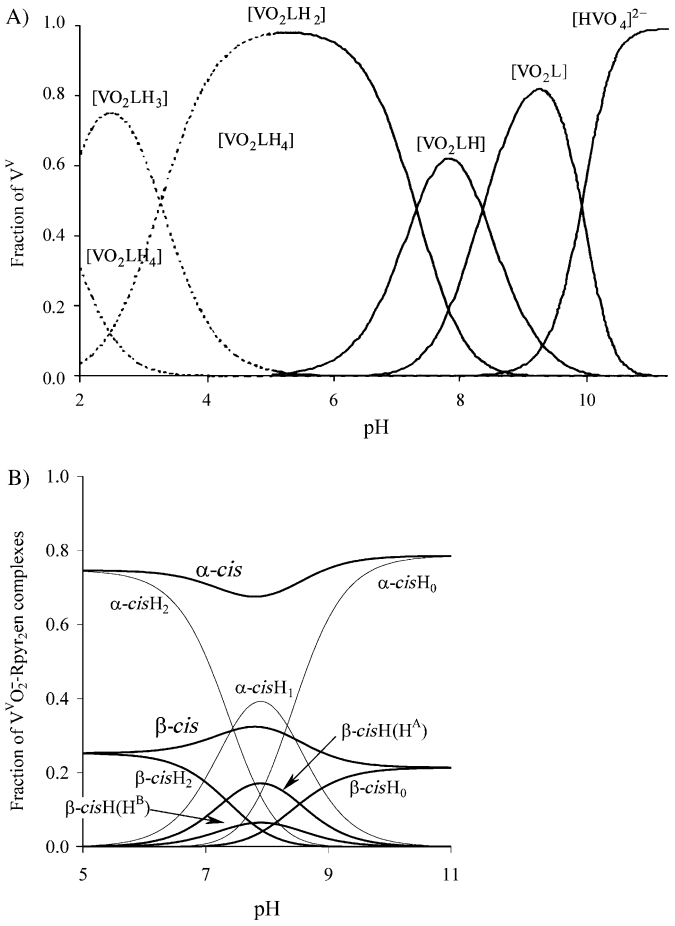

Figure 5. A) Concentration distribution curves of $V^{V}O_2$ complexes formed in solutions containing KVO_3 and H_2Rpyr_2en, with $C_V = 2.0$ mM and L:M = 2, calculated by using the stability constants listed in Table 3. At pH ~ < 4, the best fit of the potentiometric titration data was obtained with models including $[V^{V}O_2LH_3]^{2+}$ and $[V^{V}O_2LH_4]^{3+}$ in the speciation model. The color of the sample solutions turned to red parallel with the formation of $[V^{V}O_2LH_3]^{2+}$, the color then slowly faded upon decreasing the pH below 2.5. The UV/Vis measurements indicated a nonequilibrium system because of the slow formation and decomposition of this 'red-colored' species.[70] The speciation diagram for pH < 5 is therefore only approximate, and this is indicated with dashed lines. B) A microequilibrium speciation in the same conditions in the pH range 5–11.

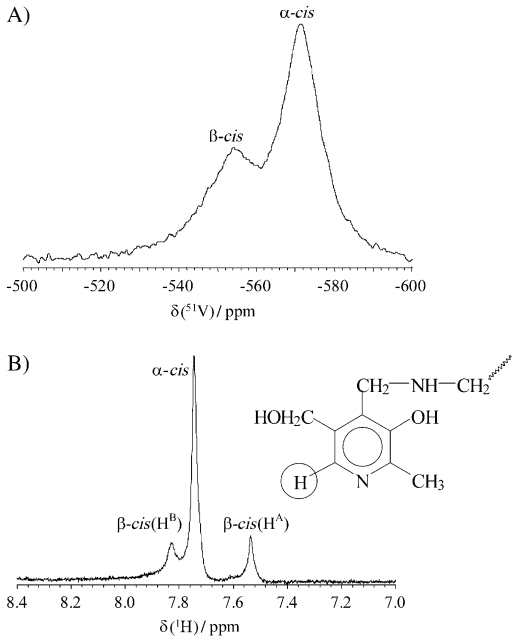

Figure 6. NMR spectra of a solution containing $NaVO_3$ and H_2Rpyr_2en with $C_V = 10$ mM and L:M = 1 at pH ~6.7. The clearly distinct $V^{V}O_2$ complexes with H_2Rpyr_2en are labeled α-*cis* and β-*cis*, which correspond to the binding modes **III** and **IV** of Scheme 2, respectively. A) ^{51}V NMR spectrum, B) ^{1}H NMR spectrum (aromatic region).

(Scheme 2) for the α-*cis* and β-*cis* complexes, respectively. While for the α-*cis* (structure **III**, which corresponds to the binding mode of complex **4**), the protons of the two half molecules are equivalent, for the β-*cis* isomer, structure **IV**, they are not. This solution structure proposed for the β-*cis* isomer was confirmed by using 2D NOESY and ROESY spectra (see SI-6 in the Supporting Information).

In the β-*cis* isomers (structure **IV**) one half of the molecule is coordinated through an O (*trans* to a O_{oxo}) and a N atom (*trans* to a $O_{phenolate}$), and this part is labeled as A; the other half of the molecule where the coordination involves O (*trans* to a N_{amine}) and N (*trans* to a O_{oxo}) is labelled as B. From the H-aromatic chemical shifts obtained in the DFT calculations (see below), for β-*cis* isomers the higher experimental H-aromatic chemical shifts (Figure 6B) correspond to part B of the molecule (see structure **IV**). The ratio of the two isomers does not change much throughout the pH range 4–10. However, due to the different acidity of the $NH^{+}_{pyridine}$ in the α-*cis* and β-*cis* isomers, there is a slight change in the ratio of the two types of isomers between pH 6 and 9, with a minimum of α-*cis*/β-*cis* at pH 7.8, where the population of the monoprotonated forms of $[VO_2LH]$ shows its maximum (Figure 5 and SI-8A in the Supporting Information).

The species involved in the microscopic deprotonation scheme of the $NH^{+}_{pyridine}$ groups of the α-*cis* and β-*cis* isomers together with the corresponding microconstants are shown in Scheme 3. Starting with $[V^{V}O_2LH_2]^{+}$ and increasing the pH, each isomer has two deprotonation steps. The first step for the α-*cis*H_2 and β-*cis*H_2 isomers can proceed by two different paths (deprotonation either on the ring A or ring B of pyridoxal), yielding either α-*cis*$H(B^H)$ or α-*cis*$H(A^H)$, and β-*cis*$H(B^H)$ or β-*cis*$H(A^H)$, respectively. As the α-*cis* isomers are symmetrical, the α-*cis*$H(B^H)$ and α-*cis*$H(A^H)$ are identical and simply represented by α-*cis*H. Therefore, theoretically there are seven different species, these being schematically depicted in Scheme 3.

Based on the pH dependence of the chemical shifts of the ^{1}H and ^{51}V NMR spectra and on the equilibria involved, the microconstants shown in Scheme 3 could be calculated (see SI-8 in the Supporting Information). The two stepwise pK_a values of α-*cis*H_2 (pK_α^{H2} and pK_α^{H1}) differ more (0.89) than the expected value based on statistical consideration (0.61). This is due to the charge of the molecule, which becomes zero after the first deprotonation. The first deprotonation of β-*cis*H_2 ($pK_\beta^{H2} = 7.19$) is lower than the pK_a of α-*cis*H_2 (7.44), and this changes the ratio of the α-*cis*:β-*cis* isomers from ~3:1 (for the stoichiometry $[VO_2LH_2]$) to ~1.7:1 (for the $[VO_2LH]$ stoichiometry). The difference in the second

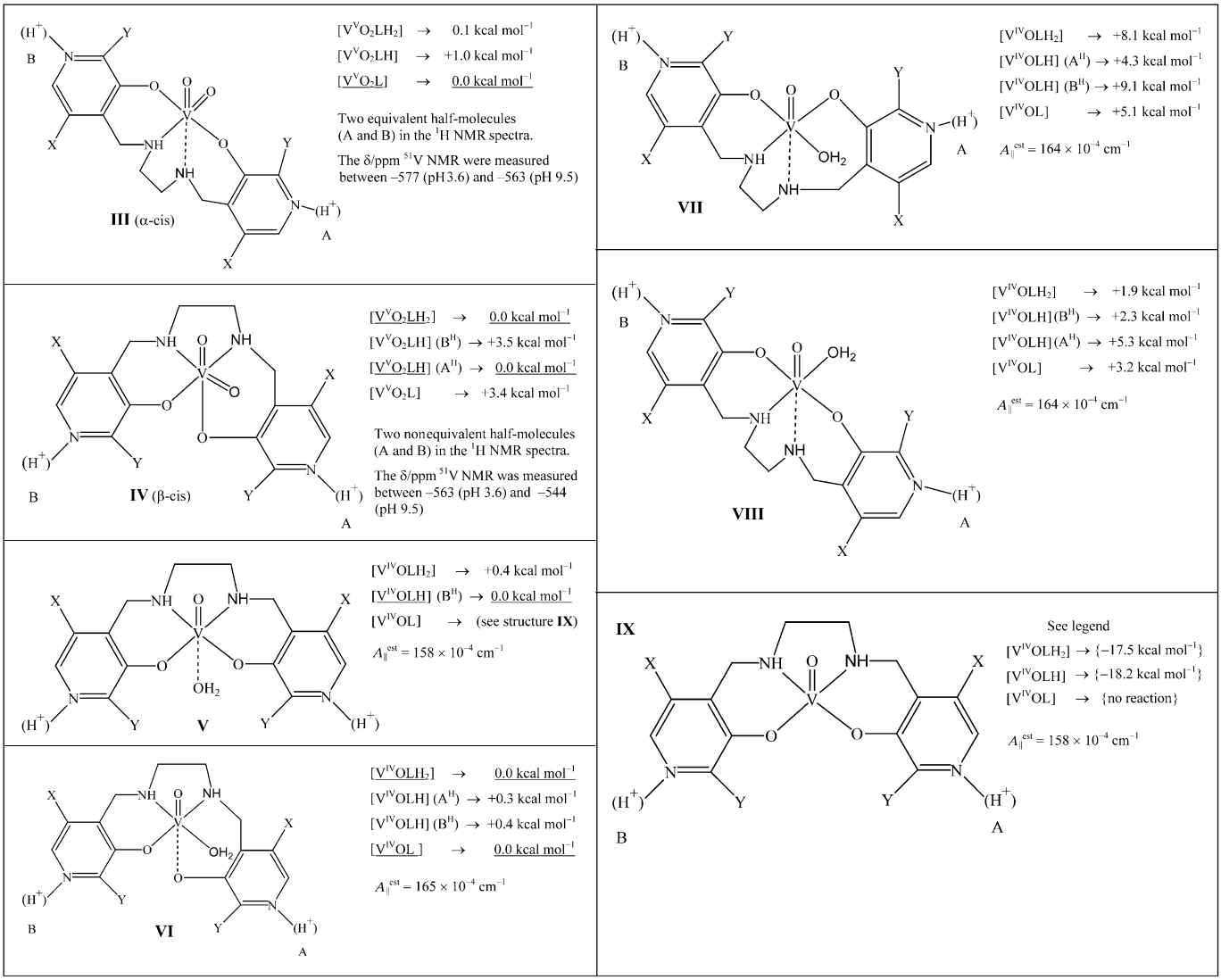

Scheme 2. Possible isomers for the $V^{V}O_2$–Rpyr$_2$en complexes (structures **III**–**IV**) and $V^{IV}O$–Rpyr$_2$en (structures **V**–**IX**), and corresponding relative energies for the structures optimized by DFT. For each of the structures **III**–**IX**, there are three stoichiometries: MLH_2 (both pyridine N atoms protonated), MLH (one of the pyridine N atoms protonated, either on side A (designated by A^H), or on side B (designated by B^H)), and ML (both pyridine N atoms deprotonated), where $M = V^{IV}O$ or $V^{V}O_2$. For *each stoichiometry* (and formal oxidation state) the isomer corresponding to the lowest energy is underlined and assigned: 0.0 kcal mol^{-1}. The energies indicated for the other isomers *of the same stoichiometry and oxidation state* are relative to the lower one. The $A_{\parallel}^{est}$ values ($V^{IV}O$ complexes) calculated using the additivity relation, the measured ^{51}V NMR chemical shifts ($V^{V}O_2$ complexes) and calculated ones (relative to $VOCl_3$) by the procedure described in the experimental section (δ_V^{cal}) are also indicated. For the five-coordinate complexes **IX** the energies indicated {in brackets} correspond to the ΔE for coordination of water. In the case of the $[V^{IV}OL]$ stoichiometry with structure **V**, this complex with coordinated water is unstable, spontaneously yielding the five-coordinate $[V^{IV}OL]$ complex with structure **IX** and free water.

stepwise deprotonation constants between the two isomers ($pK_{\alpha}^{H1} = 8.33$ and $pK_{\beta}^{H1} = 8.67$) is almost the same (0.35) as for the first (0.25), but now the pK_a of β-*cis* is higher, therefore the isomer ratio is settled back to ~3:1.

The acidity of one of the $NH^{+}_{pyridine}$ of β-*cis* is lower by ~0.42 units than the other. The assignment of the pK_{β}^{H2B} and pK_{β}^{H2A} is based on the DFT calculations. The gas-phase structure of β-*cis*H(B^H) is less stable than that of β-*cis*H(A^H) by 3.5 kcal mol^{-1}, and we assume the same trend occurs in aqueous solution. Thus the first deprotonation occurs mainly at the $NH^{+}_{pyridine(B)}$ which is more acidic, and the second deprotonation involves the $NH^{+}_{pyridine(A)}$ which is more basic. The complete resolution of the microscopic dissociation scheme, which is a good example of how the joint evaluation of parallel pH/^{1}H NMR and pH/^{51}V NMR data can be used to describe such a system revealing all fine details, is given in the Supporting Information (SI-8).

DFT calculations: Gas-phase structures are obtained by DFT calculations, but these normally give good approximations of the solution and solid-state molecular structures. The stability of the isomers is dependent on solvation and ionic interactions occurring in solution, and these environmental effects may affect the predominance of the isomers in solution. However, DFT calculations certainly may give good clues in understanding the ratio of the various binding isomers present in solution, the type of bonding present and to explain the spectroscopic properties.

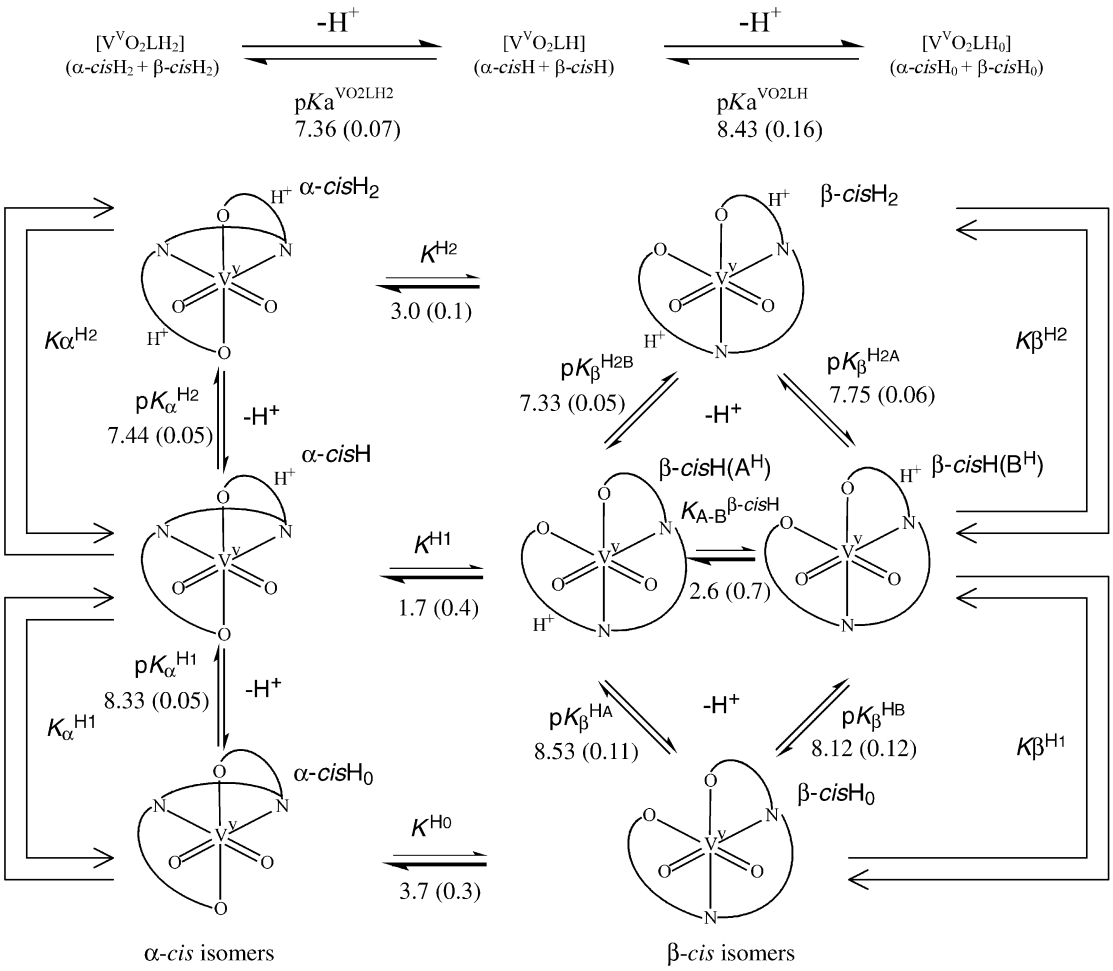

Scheme 3. The $NH^{+}_{pyridine}$ microconstant deprotonation scheme for the α-*cis* and β-*cis* isomers of $V^{V}O_2$–Rpyr$_2$enH_n complexes. The notation used is included (see also Scheme 2), as well as the pK_a values calculated from the ^{1}H and ^{51}V NMR chemical shifts for the complexes (see SI-8 in the Supporting Information). No distinct ^{51}V NMR chemical shifts could be measured or obtained for species β-*cis*H(A^H) and β-*cis*H(B^H).

DFT calculations were carried out for most of the possible isomers of diprotonated (MLH_2), monoprotonated (MLH) and deprotonated (ML) $V^{IV}O$ and $V^{V}O_2$ complexes of **2**, in order to evaluate their relative energies, to understand several aspects related to their structural preferences and electronic structure, and to determine some properties. The structure of the complexes was simplified by replacing the -CH_3 and -CH_2OH groups by -H in the pyridoxal ring. For the main objective of our calculations their effect is expected to be small, although they are relevant for intermolecular association and H-bonding interaction with solvent molecules. The Supporting Information (e.g., SI-9) summarizes the structural data, relative energies, and some properties obtained in the DFT calculations, namely the experimental and calculated ^{1}H NMR data for the isomers corresponding to **III** and **IV**.

For the $V^{IV}O$ complexes, the DFT calculations were carried out both including and excluding a coordinated H_2O ligand, revealing interesting aspects on the energetics of H_2O coordination in $V^{IV}O$ complexes. In fact, for all stoichiometries and isomers (except for one isomer and stoichiometry of the $V^{IV}O$–Rpyr$_2$en system, see below), the coordination of one H_2O molecule corresponds to an exothermic reaction with calculated ΔE between -100 and -75 kJ mol^{-1} (-24 and -18 kcal mol^{-1}). For the [V^{IV}OL] stoichiometry corresponding to structure **IX** (Scheme 2), no six-coordinate complex with a coordinated water molecule in the axial position *trans* to V=O could be obtained, all optimization attempts leading to an isolated H_2O molecule and the five-coordinate complex. This emphasizes the subtle electronic/charge effects that may be operating in this type of complex.

DFT calculations for the $V^{V}O_2$ isomers with two *trans*-O_{oxo} atoms yielded structures corresponding to energies higher (by approximately 146 kJ mol^{-1} (~35 kcal mol^{-1})) than those with two *cis*-O_{oxo} atoms. This is because while in the *cis*-$V^{V}O_2$ compounds the strongly π-donating O_{oxo} ligands have exclusive use of one d_π orbital each (d_{xz}, d_{yz}), and share a third one (d_{xy}), in the *trans*-configuration, the O_{oxo} ligands would have to share two d_π orbitals and leave one unused.

The fully optimized DFT structure (the bonding parameters are given in Table 1) corresponding to compound **4** may be used for comparison with the molecular structure determined by X-ray diffraction. As may be seen in Table 1, the calculated bond lengths and angles compare well with those for **4**. Some of the differences arise from the fact that an iso-

lated molecule was considered in the theoretical calculations, while as was revealed by X-ray diffraction, several intermolecular hydrogen bonds occur in the crystal structure of complex **4**. As for the X-ray structure, the calculated V-($O_{phenolate}$, N_{amine}) bond lengths of the half-molecule containing the protonated $NH^+_{pyridine}$ moiety are about 0.05–0.15 Å longer than in the deprotonated half-molecule.

The DFT structural data reveal that for all isomers of MLH_2, MLH and ML complexes (M = $V^{IV}O$ and V^VO_2) of **2**, in the DFT structures the (O=)V–$O_{phenolate}$(*cis*) and (O=)V–N_{amine}(*cis*) bond lengths are within the values normally found for this type of bond: approximately 1.9–2.1 and 2.1–2.25 Å, respectively, the longer distances corresponding to the cases where the group is *trans* to a $O_{phenolate}$ donor (as O4 in compound **4**). For the [$V^{IV}OLH_2$], [$V^{IV}OLH$], and [$V^{IV}OL$] complexes, five, eight, and five isomers were considered, respectively (see Scheme 2), the average V–O_{oxo} bond lengths being 1.599, 1.611, and 1.619 Å, respectively. A similar trend was observed for the V^VO_2 complexes. The longer V–O_{oxo} lengths (approximately 1.61–1.63 Å) correspond to the complexes where the O_{oxo} atom is *trans* to a $O_{phenolate}$ atom.

The (O=)V–$O_{phenolate}$(*trans*) and (O=)V–N_{amine}(*trans*) bond lengths are within the range 1.94–2.20, and 2.25–2.42 Å, respectively. For several of the more stable isomers of the $V^{IV}O$ and V^VO_2 complexes the (O=)V–$O_{phenolate}$(*trans*) bond lengths are shorter than expected,[71–75] the lower values (1.94 Å) being found for some of the $V^{IV}O$ complexes. There are only a few complexes with (O=)V–$O_{phenolate}$(*trans*) bonds with structures characterized by X-ray diffraction,[76] and the calculated (O=)V–$O_{phenolate}$(*trans*) distances are intermediate between those of the *cis* form, when the $O_{phenolate}$ is in the equatorial plane (approximately 1.9 Å), and those of the compounds containing neutral oxygen donors, including the $HO_{phenolate}$ group (approximately 2.2–2.4 Å).[73,74] Thus, the *trans* influence of the O_{oxo} ligand is still expressed when one compares the lengths ~1.9 and ~2.1 Å.

In agreement with the spectroscopic (EPR and NMR) results, the DFT calculations indicate that, for each stoichiometry [ML], [MLH], and [MLH_2] (M = $V^{IV}O$ and V^VO_2) there are several isomeric structures corresponding to similar energies. For the $V^{IV}O$ complexes the binding modes correspond to structures **V**–**IX** included in Scheme 2, and the only one that appears to be energetically disfavored corresponds to structure **VII**. Nevertheless, for each stoichiometry at least three types of isomers may exist in solution with $A_{\parallel}^{est}$ values of either 158 or 164–5×10^{-4} cm^{-1}. This is in good agreement with the experimental values (Figure 4 and Table 2), which showed the existence of two distinct signals with $A_{\parallel}$ values of 157–8 and 164–6×10^{-4} cm^{-1} in the pH range 2–8, that is, also for all stoichiometries.

For the V^VO_2 complexes all types of isomers considered in the DFT calculations (binding modes **III**–**IV** in Scheme 2) correspond to similar energies. The maximum energy difference found was 14.6 kJ mol^{-1} (3.5 kcal mol^{-1}), and this for two isomers of the [V^VO_2LH] stoichiometry with equal binding mode (structure **IV**: β-*cis*H(A^H) and β-*cis*H(B^H) in Scheme 3), and differing in the type of pyridine-N atom that is protonated.

Conclusion

The Schiff-base ligand of pyridoxal and ethylenediamine, **1**, and its hydrolytically more stable reduced derivative **2** proved to be efficient binders of both vanadium(IV) and vanadium(V). X-ray diffraction studies show the Schiff base pyr_2en and the reduced Schiff base $Rpyr_2en$ with strong intramolecular hydrogen bonds. Several $V^{IV}O$ and V^VO_2 complexes of these and related ligands were prepared and their properties studied. One of these, namely [V^VO_2(HRpy$r_2$en)], was isolated in crystalline form and structurally characterized by X-ray diffraction. Both pyr_2en and $Rpyr_2en$ were found to form basically similar complexes, the tetradentate coordination of the ligands through $2\times O_{phenolate}$ and $2\times N_{amine/imine}$ being the predominant binding mode. [$V^{IV}O$-(pyridoxaminato)$_2$] was also characterized and involves one of the vitamin B_6 forms as the ligand, the binding mode being similar.

IR and magnetic susceptibility measurements with the $V^{IV}O$ complex of the reduced SB revealed weak V=O···V=O interactions between the metal ion centers, which are not present in the corresponding complex formed with the Schiff base.

The acid–base properties of the ligands, and complexation with $V^{IV}O^{2+}$ and $V^VO_2^+$ in aqueous solution were studied by pH-potentiometry, visible absorption, EPR, ^1H and ^{51}V NMR spectroscopy. We highlight the differences in the binding abilities of the SB and its reduced derivative towards both $V^{IV}O^{2+}$ and $V^VO_2^+$, which is clearly demonstrated by the values of the proton displacement constants (K*) characteristic to the formation equilibrium: $V^{IV}O^{2+} + H_6L^{4+} \rightleftharpoons [V^{IV}OLH_2]^{2+} + 4H^+$; the log K* values are −14.1 and −5.63 for pyr_2en and $Rpyr_2en$, respectively. This difference in the stability may probably be explained by the much higher flexibility of the reduced Schiff base ligand, lacking the −C=N double bonds, thus resulting in significantly less strain and/or better ligand–metal orbital overlap in the complexes formed. The Schiff base may also hydrolyze, and this was confirmed by both solution studies and X-ray characterization of $[(V^VO_2)_2(pyren)_2]\cdot 2H_2O$, containing the half Schiff base $pyren^-$ as ligand.

EPR ($V^{IV}O$–$Rpyr_2en$ system) and ^1H and ^{51}V NMR (V^VO_2–$Rpyr_2en$ system) studies indicated the presence of various isomeric species in solution. The combined quantitative treatment of the pH-metric and spectral data provided the complete description of the equilibrium system. It was shown that distinct species result from the protonation/deprotonation of the $NH^+_{pyridine}$ of the ligand. For the V^VO_2–$Rpyr_2en$ system microequilibrium constants between seven types of complexes were calculated from the measured ^1H and ^{51}V NMR chemical shifts. DFT calculations provided sensible molecular structures, and energy values for the various isomers, confirming the assumptions made on the EPR and NMR data.

Overall the present systems are remarkable examples of the complexity of the types of isomers that may form in solutions of $V^{IV}O$ and V^VO_2 complexes (and indeed in many other metal–ligand systems), and how pH-potentiometry, spectroscopy, DFT calculations, and handling of the experi-

mental data may be used to characterize the systems in solution.

The complexes prepared are slightly soluble in water and the order of stability of the complexes formed is pyridoxamine $<$ H_2pyr_2en $<$ H_2Rpyr_2en. Pyridoxal and pyridoxamine are forms of vitamin B_6 and are nontoxic metabolites. Their vanadium complexes may therefore be good candidates for therapeutic use. Toxicity, insulin-mimetic, and other biological studies of these vanadium complexes are in progress.

Experimental Section

Materials: All chemicals used for the synthetic work were obtained from Merck, Sigma-Aldrich or Calbiochem were of reagent grade. They were used without further purification.

Synthesis of the ligands

Preparation of H_2pyr_2en (1): Pyridoxal·HCl (2.24 g, 11 mmol) was dissolved in H_2O (40 mL) and the pH was set to 6.5 by addition of concentrated KOH. Ethylenediamine (0.334 mL, 5 mmol) dissolved in ethanol (5 mL) was added dropwise to the pyridoxal suspension. The mixture was stirred under reflux for 1 h. The yellow precipitate formed was separated by filtration, washed with H_2O, ethanol, and diethyl ether, and dried under vacuum. Yield: 97%; elemental analysis calcd (%) for $C_{18}H_{22}N_4O_4$: C 60.32, H 6.19, N 15.63; found: C 60.6, H 6.3, N 15.7; MS: m/z: 358; NMR (D_2O) (pH ~ 4.3): $\delta = 2.49$ (s, 6H; CH_3), 3.31 (s, 4H; CH_2–OH), 5.1 (dd, 4H; -CH_2CH_2-), 6.58 (s, 2H; CH=N), 7.77 (s, 2H; $CH_{aromatic}$). The solution of the filtrate was kept at room temperature; after several weeks yellow crystals suitable for X-ray diffraction were collected.

Preparation of H_2Rpyr_2en (2): $NaBH_4$ (0.11 g, 3.00 mmol) dissolved in methanol containing KOH was added to a suspension of H_2pyr_2en (1.00 g, 2.79 mmol) in methanol/chloroform (3:2, 50 mL). The mixture was stirred at about 5°C overnight, and the yellow solution turned colorless. HCl (2 M) was added until pH 4–5 was reached, and the solution was stirred for 2 h. The pH was then increased to 10 by addition of KOH (3 M). The white precipitate was filtered, washed with water, ethanol, and diethyl ether, and dried under vacuum. Yield: 60%; elemental analysis calcd (%) for $C_{18}H_{26}N_4O_4$: C 59.65, H 7.23, N 15.35; found: C 59.5, H 7.3, N 15.4; NMR (D_2O) (pH ~ 4.8): $\delta = 2.41$ (s, 6H; CH_3), 3.35 (s, 4H; -CH_2CH_2-), 4.35 (s, 4H; CH_2NH), 4.63 (s, 4H; CH_2OH), 7.62 (s, 2H; $CH_{aromatic}$). From the solution of the filtrate, kept at room temperature for two weeks, colorless crystals were collected and characterized by X-ray diffraction.

Synthesis of the vanadium complexes: All reactions were carried out under a nitrogen atmosphere. The procedure for the synthesis of all $V^{IV}O$ complexes was similar: the ligand (1 equiv) was dissolved in an alcoholic solvent (or a methanol/water mixture) and sodium acetate (2 equiv) was added. Then 1.1 equivalents of the vanadium salt (either chloride or sulfate) dissolved in water were slowly added and the pH was set to 7.5–8 by addition of 3 M KOH. After precipitation of the complex, the solution was filtered, washed, and dried under vacuum.

Crystals of $[V^{V}O_2(HRpyr_2en)]$ (4): The pH of a solution containing H_2Rpyr_2en (3 mM) and KVO_3 (3 mM) was adjusted to about 7 by addition of 0.2 M KOH. After about 24 h at room temperature yellow crystals suitable for X-ray diffraction were collected.

Preparation of $[V^{IV}O(pyr_2en)]$ (5): A dark green solid was obtained. Yield: 91%; elemental analysis calcd (%) for $C_{18}H_{20}N_4O_5V{\cdot}2.4H_2O$ {formulation: $[V^{IV}O(pyr_2en)]{\cdot}2.4H_2O$}: C 46.34; H 5.36, N 12.01; found: C 46.0, H 5.2, N 11.8.

Preparation of $[V^{IV}O(Rpyr_2en)]$ (6): A pink solid was obtained. Yield: 75%; elemental analysis calcd (%) for $C_{18}H_{24}N_4O_5V{\cdot}2.5H_2O$ {formulation: $[V^{IV}O(R\text{-}pyr_2en)]{\cdot}2.5H_2O$}: C 45.77, H 6.19, N 11.86; found: C 45.5, H 6.2, N 11.6.

Preparation of $[V^{IV}O(pyrN)_2]$ (7): The ratio L:M was 2:1. A light pink precipitate was obtained. Yield: 52%; elemental analysis calcd (%) for $C_{16}H_{22}N_4O_5V{\cdot}6H_2O$ {formulation: $[V^{IV}O(pyrN)_2]{\cdot}6H_2O$}: C 37.73, H 6.73, N 11.00; found: C 37.4, H 6.6, N 10.6.

Preparation of $[V^{IV}O(Me\text{-}pyrN)_2]$ (8): The Schiff base Me-pyrN was formed in situ by reaction of pyridoxal·HCl (1 equiv) with methylamine (1 equiv). In the end an orange compound precipitated. Yield: 65%; elemental analysis calcd (%) for $C_{18}H_{22}N_4O_5V{\cdot}2.5H_2O$ {formulation: $[V^{IV}O(Me\text{-}pyrN)_2]{\cdot}2.5H_2O$}: C 45.96, H 5.79, N 11.91; found: C 46.2, H 5.9, N 11.6.

Crystals of $[(V^{V}O_2)_2(pyren)_2]{\cdot}2H_2O$ (9): After about two weeks, some crystals were formed from the filtrate obtained in the preparation of **5**, which was left in a flask and in contact with air at about 4°C. These were collected and characterized by X-ray diffraction.

Physical and spectroscopic studies: IR spectra were recorded with a BioRad FTS 3000 MX FTIR spectrometer. Visible spectra were recorded either with a Hitachi U-2000 or a Perkin-Elmer Lambda 9 UV/VIS/NIR spectrophotometer. The EPR spectra were recorded at 77 K (on glasses made by freezing solutions in liquid nitrogen) with a Bruker ESP 300E X-band spectrometer. The magnetic susceptibilities were measured in the range 5–296 K using a 7-Tesla Faraday Oxford Instruments system coupled to a Sartorius S3D-V microbalance. The ^1H and ^{51}V NMR spectra were obtained on a Varian Unity-500 NMR Spectrometer operating at 499.824, and 131.404 MHz, respectively, using a 5-mm broad band probe and a controlled temperature unit set at 25 ± 1°C. The 2D COSY, NOESY, ROESY, and TOCSY spectra were also obtained at 25 ± 1°C, on the same NMR spectrometer using the same 5-mm broad band probe.

X-ray crystal structure determination of 1, 4, and 9: For the three compounds data were collected on a MACH3 Enraf-Nonius diffractometer with Mo graphite-monochromated radiation. The crystal structures were solved by direct methods (program SIR97[77]) and refined by SHELXL97,[78] all in the package WinGX-Version 1.64.03b.[79] All non-hydrogen atoms were refined anisotropically and hydrogen atoms for **1** and **9** that were located in the Fourier maps were refined isotropically. In compound **4** the hydrogen atoms were included in calculated positions and allowed to be refined, while riding on the parent C atom, except for the nitrogen and the water hydrogen atoms, which were located and refined isotropically with some constraints. Further details of the crystal structure determinations are given in Table 4 and in the Supporting Information (SI-1). Graphical representations were prepared by using ORTEPIII[77] and SCHAKAL99.[80]

X-ray crystal structure determination of 2: Three-dimensional, room-temperature X-ray data were collected on a Siemens Smart 1000 CCD instrument. The structures were solved by direct methods and refined by full-matrix least-squares on F^2. Hydrogen atoms were left to refine freely with isotropic thermal parameters. Complex scattering factors were taken from the program package SHELXTL.[81] Details are given in Table 4 and SI-1 in the Supporting Information.

Further details of the crystal structure investigations may be obtained from the Fachinformationszentrum Karlsruhe, 76344 Eggenstein-Leopoldshafen, Germany (fax: (+49) 7247-808-666; e-mail@crysdata fiz-karlsruhe.de) on quoting the depository CSD-212900, CSD-212452, CSD-212901, and CSD-212902 for compounds **1**, **2**, **4**, and **9**, respectively.

Determination of the vanadium content in samples: A procedure was developed for this purpose (see Supporting Information SI-10).

pH-potentiometric titrations: All measurements were made in water. The purity of the ligands was checked pH-potentiometrically and the exact concentration of solutions were determined by the Gran method.[82] The stock solution of $V^{IV}O$ was prepared and standardized as reported earlier[83] and also as mentioned above. The H_3O^+ concentration in the stock solutions was determined by pH-potentiometry. The V^{V} stock solution was prepared by dissolving KVO_3 in KOH solution of known molarity and its H_3O^+ concentration was calculated. The vanadium content in the commercial KVO_3 was determined as described above.

All solutions were manipulated in an inert atmosphere (high purity N_2 or purified argon). The ionic strength was adjusted to 0.20 M KCl and the temperature was 25.0 ± 0.1°C. The pH was measured with an Orion 710 A precision digital pH meter equipped with an Orion Ross 8103BN-type combined glass electrode, calibrated for hydrogen ion concentration as described earlier.[84] The ionic product of water was $pK_w = 13.76$.

Stability constants were determined by pH-metric titration of 10.0 or 25.0 mL samples. The ligand concentrations were in the range 0.0005–0.005 M (0.0005–0.01 M for pyridoxamine), and the L:M ratio from 1 to 4 (2 to 12 for pyridoxamine). Titrations were normally done from pH 2.0

Table 4. Crystal and structure refinement data.

	H_2pyr_2en (**1**)	H_2Rpyr_2en (**2**)	$[VO_2(HRpyr2en)]\cdot 3H_2O$ (**4**)	$[(VO_2)_2(pyren)_2]\cdot 2H_2O$ (**9**)
empirical formula	$C_9H_{11}N_2O_2$	$C_{18}H_{26}N_4O_4$	$C_{18}H_{31}N_4O_9V$	$C_{10}H_{18}N_3O_6V$
formula weight	179.20	362.43	497.40	327.21
temperature [K]	293(2)	298(2)	293(2)	293(2)
wavelength [Å]	0.71073	0.71073	0.71073	0.71073
crystal system	triclinic	tetragonal	monoclinic	monoclinic
space group	$P\bar{1}$	$P4_12_12$	$P21/a$	$P21/a$
a [Å]	7.142(2)	8.7035(10)	7.131(3)	8.791(3)
b [Å]	7.897(3)	8.7035(10)	35.877(7)	13.650(6)
c [Å]	8.270(5)	24.120(4)	9.509(2)	12.347(5)
α [°]	72.76(2)	–	–	–
β [°]	80.87(2)	–	111.55(2)	109.140(3)
γ [°]	76.72(3)	–	–	–
volume [Å^3]	431.5(3)	1827.1(4)	2262.6(12)	1399.7(10)
Z	2	4	4	4
reflections collected/unique	1953/1824 [R(int) = 0.1030]	11 959/2255 [R(int) = 0.0481]	4377/4038 [R(int) = 0.1438]	2821/2696 [R(int) = 0.0850]
refinement method	full-matrix least-squares on F^2	full-matrix least-squares on F^2	full-matrix least-squares on F^2	full-matrix least-squares on F^2
goodness-of-fit on F^2	0.902	1.002	1.072	1.036
final R indices [$I > 2\Sigma(I)$]				
$R1$	0.0774	0.0417	0.0826	0.0383
$wR2$	0.0961	0.0845	0.1941	0.0912
R indices (all data)				
$R1$	0.2710	0.0716	0.1396	0.0541
$wR2$	0.1401	0.0961	0.2386	0.0993

until 11.5, unless very extensive hydrolysis, precipitation or very slow equilibration was detected, with KOH solution of known concentration (approximately 0.2 M) under a purified argon atmosphere. The reversibility of the complexation reactions with V^V was checked by back-titrations (by titrating samples from basic pH with HCl solution of known concentration (approximately 0.2 mol dm^{-3})). The reproducibility of titration points included in the evaluation was within 0.005 pH units in the whole pH range.

The concentration stability constants $\beta_{pqr} = [M_pL_qH_r]/[M]^p[L]^q[H]^r$ were calculated by using the PSEQUAD computer program.[63] The formation of the following $V^{IV}O$–hydroxo complexes was taken into account: $[V^{IV}O(OH)]^+$, $[(V^{IV}O)_2(OH)_2]^{2+}$, $[(V^{IV}O)_2(OH)_5]^-$, and $[V^{IV}O(OH)_3]^-$.[71,85,86] For the V^v systems the stability constants were similarly defined, where M refers to VO_2^+, not as HVO_4^{2-} as is most usual in the literature. The speciation of vanadate into monomeric, dimeric, tetrameric, pentameric, and decameric species[87] was taken into account (see SI-11 in the Supporting Information).

UV/Vis spectroscopy: All measurements were made in water, except a few involving the dissolution of solid complexes, mentioned in SI-3 in the Supporting Information. The temperature was kept at 25.0 ± 0.3 °C with circulating water. Unless otherwise stated, by visible (Vis) spectra we mean a representation of ε_m values versus λ [ε_m = absorption/(bC_M) where b = optical path (either 0.1 or 1 cm cells were used) and C_M = total metal concentration]. The spectral range covered was normally 350–900 nm.

The Vis spectra were recorded changing the pH with approximately fixed total vanadium and ligand concentrations. $V^{IV}O$–H_2pyr_2en system: at L:M ratios of 6:1 (C_{VO} ~4.5 mM) and 2:1 (C_{VO} ~5 mM); $V^{IV}O$–H_2Rpyr_2en system: at L:M ratios of 1:1 (C_{VO} ~5 mM) and 2:1 (C_{VO} ~4.2 mM); $V^{IV}O$–$H_2(pyrN)_2$ system: at a L:M ratio of 10:1 (C_{VO} ~3 mM). For the V^VO_2–H_2Rpyr_2en system the absorption spectra (380–900 nm) were recorded at a L:M ratio of 2:1 with two vanadate concentrations: 0.8 mM (from pH 2.0 to 11) and 3 mM (from pH 11 to 2.0).

EPR spectroscopy: In the absence of ethylene glycol a relatively broad background was present in most of the frozen solution EPR spectra, therefore most spectra were run with aqueous solutions containing 5% ethylene glycol. The $V^{IV}O$ EPR spectra were simulated using a program from Rockenbauer.[44] The EPR spectra help to elucidate which groups coordinate in solution.[45,88] For the $V^{IV}O$ systems we used the additivity rule to estimate the hyperfine coupling constant $A_{\parallel}^{est}$.[46]

^{1}H and ^{51}V NMR spectroscopy: All NMR samples were prepared at room temperature immediately before NMR spectroscopic determinations. Ligand solutions for the NMR pH titrations were prepared in D_2O (99.995% D) weighing the appropriate amount of the ligand to have the desired concentration. The pD values of these solutions were adjusted with DCl and CO_2-free NaOD solutions and measured on a Crison MicropH 2002 pH meter with an Ingold 405M5 combined electrode, calibrated at 20 ± 1 °C with standard buffers at pH 4.0 and 7.0. The final pH values were corrected for the deuterium isotope effect using pH = pD − 0.4.[89]

The solutions containing the V^v complexes were prepared by weighing an adequate amount of the ligand and dissolving it in a H_2O solution of the vanadate salt of known concentration (with 10% D_2O) to obtain ^{51}V NMR spectra, or in a D_2O solution of the V^V salt when the samples were analyzed by one-(1D) and two-dimensional (2D) ^{1}H NMR spectroscopy, to have the desired L:M ratios. Several sets of experiments as a function of pH, with different L:M ratios and total concentrations were carried out.

The ^{1}H and ^{51}V and NMR chemical shifts were referenced relative to TSS at 0 ppm and to a $VOCl_3$ external solution at 0 ppm, respectively. A presaturation pulse sequence was used for ^{1}H NMR spectra to eliminate the residual water signal. The aqueous V^V–H_2Rpyr_2en system was also studied by 2D ^{1}H NMR techniques, including COSY, NOESY, TOCSY, and ROESY, using the respective pulse sequences installed in the software of the NMR instrument. ^{51}V NMR acquisition parameters were: 33 kHz spectral width, 30 μs pulse width, 1 s acquisition time, and 10 Hz line broadening. The signal intensities of the NMR resonances were obtained using the program NUTS.[90]

Molecular orbital calculations: The calculations were performed with the B3LYP HF/DFT hybrid functional as implemented in the Gaussian 98 set of programs.[91] The functional includes a mixture of Hartree–Fock[13] exchange with DFT[14] exchange-correlation, given by Becke's three parameter functional[92] with the Lee, Yang, and Parr correlation functional, which includes both local and nonlocal terms.[93,94] All the optimized geometries are the result of full optimizations without any symmetry constraints, done with model complexes with the CH_3 and CH_2OH substituents of the pyridoxal rings replaced by hydrogen atoms.

Spin unrestricted calculations were done to optimize all the possible isomers of the $V^{IV}O$ complexes in the three protonation states (di-, mono-, and deprotonated), with and without water coordinated, in a total of 32 different species. A standard LanL2DZ basis set[95–98] was used for the optimisations. In the case of the isomers presenting two equatorial N_{amine}, two equatorial $O_{phenolate}$ and one axial H_2O, *trans* to the V=O bond (structure **V** in Scheme 2), the B3LYP optimized structures described the H_2O coordination poorly, with long V–O(water) lengths (>2.4 Å) and enhanced H(water)-$O_{phenolate}$ hydrogen interactions. Thus, the Barone and Adamo one parameter functional[99] with modified Perdew–Wang exchange and Perdew–Wang 91 correlation[100–104] (MPW1PW91) was used to re-optimize those complexes, since this functional is known to describe weak interactions better than B3LYP.[105] Indeed, the structures obtained

in this way, and discussed in the text, present shorter V–O(water) and longer H(water)–$O_{phenolate}$ separations than the ones resulting from the B3LYP optimizations. Single-point energy calculations with the B3LYP functional and a standard 6–31G(d,p) basis set[106–110] were done for all the optimized structures. Spin contamination was carefully monitored for all the unrestricted calculations performed, and the values of $<S^2>$ (0.7500–0.7501) indicate minor spin contamination.

All possible isomers in the three protonation states of the $V^{V}O_2$ complexes (in a total of 10 different species) were optimized using the B3LYP functional and a 6–31G(d,p) basis set, and their relative energies obtained by means of single point calculations performed with the same functional and a standard 6–311G(d,p) basis set.[111–117] NMR shielding tensors were calculated using the Gauge-Independent Atomic Orbital method (GIAO)[118–122] at the Hartree–Fock level using a 6–311+G(2d,p) basis set. The calculations were done for the several V^{V}–Rpyr$_2$en complexes, $VOCl_3$, VO_4^{3-}, and HVO_4^{2-}. The calculated frequencies presented in the text were scaled by a factor of 0.96.[68]

Acknowledgement

This work was carried out in the frame of a COST D21 project. The authors are grateful to A. R. Tomé for help with the use of the program Origin.6, and the financial support of the Hungarian National Research Fund (OTKA T31896/2000), Hungarian Academy of Sciences, Fundo Europeu para o Desenvolvimento Regional, Fundação para a Ciência e Tecnologia, POCTI Programme (project POCTI/35368/QUI/2000), and the Hungarian–Portuguese Intergovernmental S & T Cooperation Programme for 2000–2001.

[1] S. W. Taylor, B. Kammerer, E. Bayer, *Chem. Rev.* **1997**, *97*, 333.
[2] R. E. Berry, E. M. Amstrong, R. L. Beddoes, D. Collison, S. N. Ertok, M. Helliwell, C. D. Garner, *Angew. Chem.* **1999**, *111*, 871; *Angew. Chem. Int. Ed.* **1999**, *38*, 795.
[3] T. Ishii, I. Nakai, C. Numako, K. Ohoshi, K. Otake, *Naturwissenschaften* **1999**, *80*, 268.
[4] a) I. Harvey, J. M. Arber, R. R. Eady, B. E. Smith, C. D. Garner, S. S. Hasnain, *Biochem. J.* **1990**, *266*, 929; b) J. Chen, J. Cristiansen, R. C. Titsworth, B. J. Hales, S. J. George, *J. Am. Chem. Soc.* **1993**, *115*, 929.
[5] S. Macedo-Ribeiro, W. Hemrika, R. Revirie, R. Wever, A. Messerschimdt, *J. Biol. Inorg. Chem.* **1999**, *4*, 209.
[6] A. N. Antipov, D. Y. Sorokin, N. P. L'Lov, J. G. Kuenen, *Biochem. J.* **2003**, *369*, 185–189.
[7] A. N. Antipov, N. M. Lyalikova, T. V. Khilniak, N. P. L'Lov, *FEBS Lett.* **1998**, *441*, 257–260.
[8] a) K. H. Thompson, J. H. McNeill, C. Orvig, *Chem. Rev.* **1999**, *99*, 2561–2571b) K. H. Thompson, C. Orvig, *J. Chem. Soc. Dalton Trans.* **2000**, 2885–2892.
[9] A. E. Evangelou, *Crit. Rev. Oncol. Hematol.* **2002**, *42*, 249–265.
[10] D. Rehder, J. Costa Pessoa, C. F. G. C. Geraldes, M. M. C. A. Castro, T. A. Kabanos, T. Kiss, B. Meier, G. Micera, L. Pettersson, M. Rangel, A. Salifoglou, I. Turel, D. Wang, *J. Biol. Inorg. Chem.* **2002**, *7*, 384–396.
[11] N. Durai, G. Saminathan, *J. Clin. Biochem. Nutr.* **1997**, *22*, 31–39.
[12] J. M. Lacoste, J. Duhault , D. Ravel, EUR Pat. Appl. EP 521,787, **7-1-1993**.
[13] W. J. Hehre, L. Radom, P. V. R. Schleyer, J. A. Pople, *Ab Initio Molecular Orbital Theory*, Wiley, New York **1986**.
[14] R. G. Parr, W. Yang, *Density Functional Theory of Atoms and Molecules*, Oxford University Press, New York **1989**.
[15] N. P. Pahor, M. Calligaris, D. Nardin, L. Randaccio, *Acta Crystallogr. Sect. B* **1978**, *34*, 1360.
[16] A. Palmer, F. Brisse, *Acta Crystallogr. Sect. B* **1980**, *36*, 1447.
[17] F. H. Allen, *Acta Crystallogr. Sect. B* **2002**, *58*, 380.
[18] D. C. Crans, A. D. Keramidas, M. Moharoof-Tahir, O. P. Anderson, M. M. Miller, *Inorg. Chem.* **1996**, *35*, 3599–3606.
[19] C. J. Carrano, C. M. Nunn, R. Quan, J. A. Bonadies, V. L. Pecoraro, *Inorg. Chem.* **1990**, *29*, 944–951.
[20] M. Mahroof-Thair, A. D. Keramidas, D. Goldfarb, O. P. Anderson, M. M. Miller, D. C. Crans, *Inorg. Chem.* **1997**, *36*, 1657.
[21] G. Suss-Fink, S. Stanislas, G. B. Shul'pin, G. V. Nizova, H. Stoeckli-Evans, A. Neels, C. Bobillier, S. Claude, *J. Chem. Soc. Dalton Trans.* **1999**, 3169.
[22] S. Ulvenlund, A. S. Georgopoulou, D. M. P. Mingos, I. Baxter, S. E. Lawrence, A. J. P. White, D. J. Williams, *J. Chem. Soc. Dalton Trans.* **1998**, 1869.
[23] D. C. Crans, A. D. Keramidas, S. S. Amim, O. Anderson, S. M. Miller, *J. Chem. Soc. Dalton Trans.* **1997**, 2799.
[24] W. R. Scheidt, R. Countryman, J. L. Hoard, *J. Am. Chem. Soc.* **1971**, *93*, 3878–3882.
[25] G. J. Colpas, B. J. Hamstra, J. W. Kampf, V. L. Pecoraro, *Inorg. Chem.* **1994**, *33*, 4669–4675.
[26] C. R. Cornman, G. J. Colpas, J. D. Hoeschele, J. Kampf, V. L. Pecoraro, *J. Am. Chem. Soc.* **1992**, *114*, 9925–9933.
[27] S. Mondal, S. P. Rath, S. Dutta, A. Chakravorty, *J. Chem. Soc. Dalton Trans.* **1996**, 99–103.
[28] J. A. Bonadies, W. M. Butler, V. L. Pecoraro, C. J. Carrano, *Inorg. Chem.* **1987**, *26*, 1218–1222.
[29] X. Li, M. S. Lah, V. L. Pecoraro, *Inorg. Chem.* **1988**, *27*, 4657.
[30] L. M. Mokry, C. J. Carrano, *Inorg. Chem.* **1993**, *32*, 6119–6121.
[31] C. A. Root, J. D. Hoeschele, C. R. Cornman, J. W. Kampf, V. L. Pecoraro, *Inorg. Chem.* **1993**, *32*, 3855–3861.
[32] I. J. Bruno, J. C. Cole, P. R. Edgington, M. Kessler, C. F. Macrae, J. Pearson, R. Taylor, *Acta Crystallogr. Sect. B* **2002**, *58*, 389.
[33] C. P. Rao, A. Sreedhara, P. V. Rao, M. B. Verghese, K. Rissanen, E. Kolehmainen, N. K. S. M. A. Lokanath, J. S. Prasad, *J. Chem. Soc. Dalton Trans.* **1998**, 2383.
[34] X. Li, M. S. Lah, V. L. Pecoraro, *Inorg. Chem.* **1988**, *27*, 4657–4664.
[35] D. H. Williams, I. Fleming in *Spectroscopic Methods in Organic Chemistry*, McGraw-Hill, London **1995**, p. 42–49.
[36] K. Nakamoto in *Infrared and Raman Spectra of Inorganic* Compounds, Part B, 5th ed., Wiley, New York, **1997**, p. 73–271.
[37] G. Socrates in *Infrared and Raman Characteristic Group Frequencies. Tables and Charts*, Wiley, Chichester, **2001**, p. 108–113.
[38] R. M. Silverstein, G. C. Bassler, T. C. Morril in *Spectrometric Identification of Organic Compounds*, Wiley, New York **1991**, p. 122–125.
[39] J. R. Zamian, E. R. Dockal, G. Castellano, G. Oliva, *Polyhedron* **1995**, *14*, 2411–2418.
[40] B. Bosnich, *J. Am. Chem. Soc.* **1968**, *90*, 627–632.
[41] M. Gullotti, A. Pasini, P. Fantucci, R. Ugo, R. D. Gillard, *Gazz. Chim. Ital.* **1972**, *102*, 853–892.
[42] H. E. Smith, J. R. Neergaard, E. P. Burrows, F. M. Chen, *J. Am. Chem. Soc.* **1974**, *96*, 2908–2916.
[43] K. S. Patel, G. A. Kolawole, A. Earnshaw, *J. Inorg. Nucl. Chem.* **1981**, *43*, 3107–3112.
[44] A. Rockenbauer, L. Korecz, *Appl. Magn. Reson.* **1996**, *10*, 29.
[45] N. D. Chasteen in *Biological Magnetic Resonance* (Eds.: J. Lawrence, L. J. Berliner, J. Reuben), Plenum, New York **1981**.
[46] For the $V^{IV}O$ systems we used the additivity rule to estimate the hyperfine coupling constant $A_{\parallel}^{est}$, based on the contributions $A_{\parallel,i}$ of each of the four equatorial donor groups [$A_{\parallel}^{est} = \Sigma\ A_{\parallel,i}$ (i=1–4)]. The estimated accuracy of $A_{\parallel}^{est}$ is $\pm 3\times10^{-4}$ cm^{-1}.[45] This data can be used to establish the most probable binding mode of the complexes formed, but care must be taken as the contributions of the donor groups to the hyperfine coupling may depend on their orientation,[47] or charge of the ligand.[48] The influence of the axial donor groups (if any) is not taken into account.
[47] T. S. Smith, C. A. Root, J. W. Kampf, P. G. Rasmussen, V. L. Pecoraro, *J. Am. Chem. Soc.* **2000**, *122*, 767–775.
[48] A. J. Tasiopoulos, A. N. Troganis, A. E. Evangelou, C. P. Raptopoulou, A. Terzis, Y. Deligiannakis, T. A. Kabanos, *Chem. Eur. J.* **1999**, *5*, 910–921.
[49] C. R. Cornman, K. M. Geiser-Bush, S. P. Rowley, P. D. Boyle, *Inorg. Chem.* **1997**, *36*, 6401–6408.
[50] C. R. Cornman, E. P. Zovinka, Y. D. Boyajian, K. M. Geiser-Bush, P. D. Boyle, P. Singh, *Inorg. Chem.* **1995**, *34*, 4213–4219.

[51] B. J. Hamstra, L. P. Houseman, G. J. Colpas, J. W. Kampf, R. Lobrutto, W. D. Frasch, V. L. Pecoraro, *Inorg. Chem.* **1997**, *36*, 4866–4874.
[52] P. W. Selwood, *Magnetochemistry*, Interscience, New York **1956**, p. 78.
[53] Y. Kuge, S. Yamada, *Inorg. Chim. Acta* **1977**, *21*, 85.
[54] K. S. Patel, G. A. Kolawole, *J. Coord. Chem.* **1982**, *11*, 231–237.
[55] M. Tsuchimoto, N. Yoshioka, *Chem. Phys. Lett.* **1998**, *297*, 115–120.
[56] D. L. Huges, U. Kleinkes, G. J. Leigh, M. Maiwald, J. R. Sanders, C. Sudbrake, *J. Chem. Soc. Dalton Trans.* **1994**, 2457–2466.
[57] R. J. Motekaitis, A. E. Martell, *Inorg. Chem.* **1988**, *27*, 2718–2724.
[58] F. Lloret, J. Moratal, J. Faus, *J. Chem. Soc. Dalton Trans.* **1983**, 1743–1748.
[59] J. A. Bonadies, W. M. Butler, V. L. Pecoraro, C. J. Carrano, *Inorg. Chem.* **1987**, *26*, 1218.
[60] Z. Liu, F. C. Anson, *Inorg. Chem.* **2000**, *39*, 274.
[61] Z. Liu, F. C. Anson, *Inorg. Chem.* **2001**, *40*, 1329–1333.
[62] E. Leporati, *Anal. Chim. Acta* **1985**, *170*, 287–293.
[63] L. Zekany, I. Nagypal in *Computational Methods for the Determination of Stability Constants* (Ed.: D. Leggett), Plenum, New York, **1985**.
[64] D. E. Metzler, E. E. Snell, *J. Am. Chem. Soc.* **1955**, *77*, 2431–2437.
[65] J. Sudmeier, C. N. Reilley, *Anal. Chem.* **1964**, *36*, 1698–1706.
[66] D. E. Metzler, *J. Am. Chem. Soc.* **1957**, *79*, 485.
[67] B. H. Jo, V. Nair, L. Davis, *J. Am. Chem. Soc.* **1977**, *99*, 4467–4470.
[68] J. B. Foresman, M. J. Frisch, *Exploring Chemistry with Electronic Structure Methods*, 2nd ed. Gaussian Inc., Pittsburgh **1996**.
[69] S. S. Amin, K. Cryer, B. Zhang, S. K. Dutta, S. S. Eaton, O. P. Anderson, S. M. Miller, B. A. Reul, S. M. Brichard, D. C. Crans, *Inorg. Chem.* **2000**, *39*, 406–416.
[70] Moreover, EPR signals could also be detected in this pH range, indicating the formation of small amounts (5–10% after 48 h) of $V^{IV}O$ species, formed through the partial reduction of the metal ion. New peaks appear in the ^{1}H and ^{51}V NMR spectra, but these are broader than those at higher pH, and the assignment of the ^{1}H NMR signals becomes extremely complex, even in the aromatic region. However, no peaks are detected in the ^{51}V NMR below $|-540$ ppm$|$, which could suggest the presence of monooxovanadium(V) complexes.[25] Adding acid or base to decrease or increase the pH in the range 2–5, the observed NMR, EPR, and UV/Vis spectra show the same profile. For pH > 5 the ^{1}H and ^{51}V NMR spectra of these samples did not differ from those recorded with similar solutions that had been studied at low pH. We are currently investigating the processes involved in the $V^{IV,V}$–Rpyr$_2$en system in this pH range.
[71] L. F. Vilas-Boas, J. Costa Pessoa in *Comprehensive Coordination Chemistry, Vol 3* (Eds.: G. Wilkinson, R. D. Gillard, J. A. McCleverty), Pergamon Press, Oxford **1987**, p. 453–583.
[72] C. R. Cornman, J. Kampf, M. S. Lah, V. L. Pecoraro, *Inorg. Chem.* **1992**, *31*, 2035–2043.
[73] S. P. Rath, K. K. Rajak, A. Chakravorty, *Inorg. Chem.* **1999**, *38*, 4376–4377.
[74] C. R. Cornman, J. Kampf, V. L. Pecoraro, *Inorg. Chem.* **1992**, *31*, 1981–1983.
[75] B. Baruah, S. Das, A. Chakravorty, *Inorg. Chem.* **2002**, *41*, 4502–4508.
[76] In $[V^{V}O(salimh)(cat)]$ (salimh = 4-(2-(salicylideneamino)ethyl)imidazole, cat = catechol) the $V{-}O_{phenolate}$(*cis*) and $V{-}O_{phenolate}$(*trans*) are 1.898 and 2.193 Å, respectively,[74] in $[V^{V}O(psal)(tcat)]$ (psal = N-salicylidene-2-picolylaminato, H_2L = 3,5-di(*tert*-butyl)catechol) these are 1.861 and 2.134 Å, respectively,[75] and in $V^{IV}O(salimh)_2$ the $V{-}O_{phenolate}$(*trans*) is 2.091 Å.[74]
[77] L. J. Farrugia, *J. Appl. Crystallogr.* **1997**, *30*, 565.
[78] G. M.Sheldrick, SHELXL-97, A program for refining crystal structures, **1997**.
[79] L. J. Farrugia, *J. Appl. Crystallogr.* **2002**, ##*35*##*32*, 837.
[80] E. Keller, SCHAKAL99, Graphical representation of molecular models, **1999**, University of Freiburg, Freiburg, Germany.
[81] G. M. Sheldrick, SHELXTL, Bruker Analytical X-ray system, [release 5.1], **1997**, Madison, WI.
[82] G. Gran, *Acta Chem. Scand.* **1950**, *4*, 559.
[83] I. Nagypál, I. Fábián, *Inorg. Chim. Acta* **1982**, *61*, 109.
[84] J. Costa Pessoa, T. Gajda, R. D. Gillard, T. Kiss, S. M. Luz, J. J. G. Moura, I. Tomaz, J. P. Telo, I. Torok, *J. Chem. Soc. Dalton Trans.* **1998**, 3587.
[85] A. Komura, M. Hayashi, H. Imanaga, *Bull. Chem. Soc. Jpn.* **1977**, *50*, 2927.
[86] R. P. Henry, P. C. H. Mitchell, J. E. Prue, *J. Chem. Soc. Dalton Trans.* **1973**, 1156–1159.
[87] L. Pettersson, B. Hedman, I. Andersson, N. Ingri, *Chimica Scripta* **1983**, *22*, 254–264.
[88] I. Sóvágó, D. Sanna, A. Dessi, K. Várnagy, G. Micera, *J. Inorg. Biochem.* **1996**, *63*, 99–117.
[89] P. K. Glasoe, F. A. Long, *J. Phys. Chem.* **1960**, *64*, 188–190.
[90] NUTS-NMR data processing software, **1999**, Acorn NMR.
[91] M. J. Frisch, G. W. Trucks, R. E. Stratmann, H. B. Schlegel, J. C. Burant, G. E. Scuseria, S. Dapprich, M. A. Robb, J. R. Cheeseman, V. G. Zakrzewski, J. M. Millam, A. D. Daniels, K. N. Kudin, M. C. Strain, O. Farkas, J. Tomasi, V. Barone, M. Cossi, R. Cammi, B. Mennucci, C. Pomelli, C. Adamo, S. Clifford, J. Ochterski, G. A. Petersson, P. Y. Ayala, Q. Cui, K. Morokuma, D. K. Malick, A. D. Rabuck, K. Raghavachari, J. B. Foresman, J. Cioslowski, J. V. Ortiz, A. G. Baboul, B. B. Stefanov, G. Liu, A. Liashenko, P. Piskorz, I. Komaromi, R. Gomperts, R. L. Martin, D. J. Fox, T. Keith, M. A. Al-Laham, C. Y. Peng, A. Nanayakkara, C. Gonzalez, M. Challacombe, P. M. W. Gill, B. Johnson, W. Chen, M. W. Wong, J. L. Andres, C. Gonzalez, M. Head-Gordon, E. S. Replogle, J. A. Pople, *Gaussian 98*, *Revision A.7*, Gaussian, Inc., Pittsburgh PA **1998**.
[92] A. D. Becke, *J. Chem. Phys.* **1993**, *98*, 5648.
[93] C. Lee, W. Yang, R. G. Parr, *Phys. Rev. B* **1988**, *37*, 785.
[94] B. Miehlich, A. Savin, H. Stoll, H. Preuss, *Chem. Phys. Lett.* **1989**, *157*, 200.
[95] T. H. Dunning, Jr., P. J. Hay, *Modern Theoretical Chemistry, Vol. 3* (Ed.: H. F. Schaefer), Plenum, New York **1976**, p. 1.
[96] P. J. Hay, W. R. Wadt, *J. Chem. Phys.* **1985**, *82*, 270.
[97] W. R. Wadt, P. J. Hay, *J. Chem. Phys.* **1985**, *82*, 284.
[98] P. J. Hay, W. R. Wadt, *J. Chem. Phys.* **1985**, *82*, 2299.
[99] C. Adamo, V. Barone, *Chem. Phys. Lett.* **1997**, *274*, 242.
[100] K. Burke, J. P. Perdew, Y. Wang, *Electronic Density Functional Theory: Recent Progress and New Directions* (Eds.: J. F. Dobson, G. Vignalr, M. P. Das) Plenum, **1998**.
[101] J. P. Perdew, *Electronic Structure of Solids '91* (Eds.: P. Ziesche, H. Eschrig), Akademie Verlag, Berlin **1991**, p. 11.
[102] J. P. Perdew, J. A. Chevary, S. H. Vosko, K. A. Jackson, M. R. Pederson, D. J. Singh, C. Fiolhais, *Phys. Rev. B* **1992**, *46*, 6671.
[103] J. P. Perdew, J. A. Chevary, S. H. Vosko, K. A. Jackson, M. R. Pederson, D. J. Singh, C. Fiolhais, *Phys. Rev. B* **1993**, *48*, 4978.
[104] J. P. Perdew, K. Burke, Y. Wang, *Phys. Rev. B* **1996**, *54*, 16533.
[105] S. Tsuzuki, H. P. Lüthi, *J. Chem. Phys.* **2001**, *114*, 3949.
[106] R. Ditchfield, W. J. Hehre, J. A. Pople, *J. Chem. Phys.* **1971**, *54*, 724.
[107] W. J. Hehre, R. Ditchfield, J. A. Pople, *J. Chem. Phys.* **1972**, *56*, 2257.
[108] P. C. Hariharan, J. A. Pople, *Mol. Phys.* **1974**, *27*, 209.
[109] M. S. Gordon, *Chem. Phys. Lett.* **1980**, *76*, 163.
[110] P. C. Hariharan, J. A. Pople, *Theor. Chim. Acta* **1973**, *28*, 213.
[111] A. D. McClean, G. S. Chandler, *J. Chem. Phys.* **1980**, *72*, 5639.
[112] R. Krishnan, J. S. Binkley, R. Seeger, J. A. Pople, *J. Chem. Phys.* **1980**, *72*, 650.
[113] A. J. H. Wachters, *J. Chem. Phys.* **1970**, *52*, 1033.
[114] P. J. Hay, *J. Chem. Phys.* **1977**, *66*, 4377.
[115] K. Raghavachari, G. W. Trucks, *J. Chem. Phys.* **1989**, *91*, 1062.
[116] R. C. Binning, L. A. Curtiss, *J. Comput. Chem.* **1990**, *11*, 1206.
[117] M. P. McGrath, L. Radom, *J. Chem. Phys.* **1991**, *94*, 511.
[118] K. Wolinski, J. F. Hilton, P. Pulay, *J. Am. Chem. Soc.* **1990**, *112*, 8251.
[119] J. L. Dodds, R. McWeeny, A. Sadlej, *Mol. Phys.* **1980**, *41*, 1419.
[120] R. Ditchfield, *Mol. Phys.* **1974**, *27*, 789.
[121] R. McWeeny, *Phys. Rev.* **1962**, *126*, 1028.
[122] F. London, *Radium (Paris)* **1937**, *8*, 397.

Received: July 9, 2003
Revised: November 11, 2003 [F5317]

